World Electric Vehicle Journal

MDPI

Review

Motion Recovery After Steer by Wire Failure in Independently Actuated Electric Vehicles

Liancheng Zheng [1,2,*], Rizauddin Ramli [2,*] and Liguo Chen [1]

[1] School of Mechanical Engineering, Shandong Huayu University of Technology, Dezhou 253034, China
[2] Department of Mechanical and Manufacturing Engineering, Faculty of Engineering and Built Environment, Universiti Kebangsaan Malaysia, Bangi 43600, Malaysia
* Correspondence: zlc@huayu.edu.cn (L.Z.); rizauddin@ukm.edu.my (R.R.)

Abstract

Steering failure changes both the vehicle dynamics and the actuators available for recovery. This review examines fault diagnosis, force allocation, and motion adaptation in independently actuated electric vehicles. Recovery depends on the mechanical state left by the fault: a locked steering angle constrains wheel orientation, whereas loss of steering torque leaves the mechanism responsive to tire forces and steering geometry. Published vehicle tests show that rear steering can compensate selected fixed-angle failures, but its effectiveness decreases when unpowered front wheels move unintentionally. Differential steering has also maintained lane-change tracking on a scaled demonstrator with known actuator-state information. Simulation studies cover more severe maneuvers and fault combinations; their tracking improvements do not establish road-corridor containment. The review therefore separates tracking accuracy, yaw and sideslip stability, and vehicle-footprint clearance. It also distinguishes static force limits from forces reachable within the available recovery time. Comparisons identify the physical hardware tested, the fault information supplied to the controller, and the remaining error after compensation. The evidence supports steering-function continuation in specified test conditions. Continued travel and controlled stopping require additional assessment of diagnosis delay, low-speed steering behavior, sustained actuator capacity, and road clearance.

Keywords: steer-by-wire; fault-tolerant control; differential steering; electric vehicle; control allocation; rear-wheel steering; trajectory replanning; actuator redundancy

Check for updates

Academic Editor: Joeri Van Mierlo

Received: 4 November 2026
Revised: 19 November 2026
Accepted: 25 November 2026
Published: 28 November 2026

Copyright: © 2026 by the authors. Published by MDPI on behalf of the World Electric Vehicle Association. Licensee MDPI, Basel, Switzerland. This article is an open access article distributed under the terms and conditions of the Creative Commons Attribution (CC BY) license.

1. Introduction

A steering failure can leave an electric vehicle with substantial propulsion and braking capability but insufficient authority to follow its intended path. In independently actuated vehicles, healthy motors contribute to recovery through their effects on body motion and the steering mechanism. Usable authority varies with speed, steering state, and the time available before a road boundary is reached. These relationships make steering failure a vehicle dynamics problem as well as an actuator reliability problem [1–3].

Steer-by-wire removes the direct mechanical command path between the handwheel and the road wheels. Electronic control determines road-wheel angle and, where provided, handwheel feedback. This arrangement supports variable steering characteristics and integration with automated driving. It also changes the consequences of electrical faults. A failure may reduce motor torque, freeze a commanded angle, corrupt angle feedback, or disconnect the drive while leaving the rack mechanically free. Reviews describe progress in

steering architecture, tracking, and disturbance rejection [4,5]. Recovery analysis connects these developments to the distinct mechanical conditions produced by each failure.

Independent wheel actuation creates useful alternatives. Unequal longitudinal forces can generate a body yaw moment. Under suitable steering geometry, they can also turn an unpowered steering mechanism through forces acting about the steering axis. Rear-wheel steering supplies lateral force through a separate axle. Friction brakes remain useful when motor torque is restricted. Early reconfigurable steering and yaw-control studies established the value of these substitutions, and subsequent work incorporated stronger vehicle models and explicit actuator constraints [6–8]. The central question is which motion these actuators can produce after a particular failure.

The physical substitution predates recent predictive controllers. Dominguez-Garcia et al. [9] proposed backup steering through selective braking after disconnecting the primary actuator. Mihály and Gáspár [10] used a linear parameter-varying controller and constrained wheel-torque allocation to replace lost steering-generated yaw action in CarSim. Zhang et al. [11] combined predictive trajectory control, differential-drive steering, and direct yaw-moment allocation for complete steer-by-wire failure. These works establish distinct routes from wheel actuation to steering recovery; later studies refine their fault models, constraints, and validation.

A locked steering mechanism and a mechanism that has lost steering torque illustrate the distinction. The first retains a nearly fixed geometric orientation. The second can move under self-aligning torque, longitudinal-force moments, friction, and compliance. A controller that assumes a fixed angle may mispredict the second case even when its wheel-torque commands are accurate. Recent comparative work evaluated both conditions using rear steering, torque vectoring, and coordinated actuation, including vehicle experiments [12]. Differential-braking capability has also been examined across negative and positive kingpin offsets [13]. Together, these studies bring mechanical details into a literature often organized around controller families.

This review examines the connection between steering fault mechanics and recoverable motion in passenger-car-scale electric vehicles with independently controllable wheel torques. Four-wheel steering platforms clarify the role of additional steering authority. Off-road studies are included where they distinguish motor degradation that permits local compensation from faults requiring differential steering [14]. Motor design, road-feel synthesis, energy management, and tire estimation are considered where they affect remaining steering authority. The analysis distinguishes nominal tracking, component fault compensation, and vehicle motion recovery.

This is a selective narrative review of steering-failure recovery, with coverage through September 2026. Table 1 compares seven earlier reviews with the present synthesis [1–5,15,16]. Stolte [16] already organizes actuator fault-tolerant motion control by actuator topology, degradation, control approach, and validation. Mortazavizadeh et al. [2] review steer-by-wire components, motor drives, control, and reliability, while Perdana et al. [5] compare steering-control strategies. The present review builds on those classifications. Its narrower focus is the link between the mechanical state after steering failure and the motion that surviving actuators can recover. It updates this comparison with evidence through September 2026 and relates locked versus unpowered steering, time-dependent actuation, diagnosis and transfer assumptions, and measured recovery outcomes. It separates steering-angle tracking, vehicle stability, and road containment.

Three outcomes are assessed separately. Tracking accuracy measures position, heading, or steering-angle error relative to a stated reference. Stability concerns bounded yaw and sideslip responses under the tested conditions. Road-corridor containment requires the complete vehicle footprint to remain within the permitted boundaries throughout the transition.

A lower RMS tracking error does not establish either of the other outcomes. Replanning can increase deviation from the original reference while improving road containment.

Table 1. Scope of related reviews and the present synthesis.

Review	Organizing Scope	Relation to the Present Synthesis
Huang et al. [1]	Steer-by-wire fault tolerance, architecture, and control	Provides subsystem methods; this review relates retained mechanical state to vehicle recovery.
Mortazavizadeh et al. [2]	Steering history, components, motor drives, advanced control, and reliability	Provides architecture and reliability context; this review follows the post-fault motion transition.
Hang and Chen [3]	Independent drive/steering configurations and vehicle control	Provides actuator configurations; this review compares the authority retained after steering failure.
Lu et al. [4]	Development and control of steer-by-wire systems	Provides steering-system context; this review separates local angle tracking from vehicle recovery.
Perdana et al. [5]	Control strategies for steer-by-wire systems	Provides a controller-oriented comparison; this review organizes results by fault mechanics and validation.
Stolte [16] 2021 preprint survey	Actuator topology, steering/drive/brake degradations, control approaches, and experimental validation	Closest prior classification. This review narrows the scope to steering-failure recovery, updates evidence through September 2026, and links fault mechanics to reachable forces, transfer timing, and measured outcomes.
Huang et al. [15]	Torque allocation for stability and energy efficiency	Provides allocation methods; this review examines the changed force reserve after steering failure.
Present review	Motion recovery after steering failure	A focused synthesis of mechanical state, time-dependent authority, diagnostic transition, and tracking/stability/containment evidence.

The following sections examine fault mechanics, achievable forces, diagnosis, actuator coordination, and reference adaptation. The evidence assessment then relates reported outcomes to validation platforms and recovery conditions. Successful recovery is defined here as feasible motion through the transition, with road containment and a terminal state suitable for stable continuation or stopping.

2. Steering Failure States and Recovery Mechanisms

2.1. What Remains After the Steering Actuator Fails

A steering fault model specifies the behavior retained by the failed hardware. After power loss, friction may hold the mechanism near its last position, while a backdrivable mechanism responds to tire forces. A mechanical jam holds an angle despite a command to return to zero. Saturation preserves commands within the available range. Table 2 maps both road-wheel faults and upstream input, feedback, controller, and communication faults to the behavior required in a recovery model [1,2,5,16]. Figure 1 illustrates three common road-wheel states. Upstream faults are included because their eventual mechanical state depends on isolation and the implemented fail-state.

Partial effectiveness is commonly modeled by multiplying commanded actuator torque by a factor between zero and one and adding a bias or disturbance. This formulation supports adaptive compensation and observer design [17,27]. Reduced torque constant, current limitation, and added friction can produce similar angle errors but differ in reversibility, rate dependence, and thermal behavior. Relating the estimated effectiveness to an admissible torque range preserves these physical differences in the recovery controller.

Table 2. Steering fault states and their implications for recovery.

Fault Type	Time Evolution	Retained Physical Behavior	Recovery Action and Limiting Condition
Reduced effectiveness	Abrupt, progressive, or intermittent	Reduced steering torque for a given command	Local compensation or auxiliary actuation; current and thermal reserve [17,18]
Steering lock	Persistent or intermittent engagement	Wheel/rack angle constrained at the lock value	Rear steering or wheel-force redistribution; lock angle and asymmetric tire demand [12,19]
Loss of steering torque	Abrupt or intermittent power/torque loss	Unpowered mechanism can move under road forces	Differential steering, rear steering, and yaw control; backdrivability and steering geometry [13,20]
Restricted angle range	Fixed, changing, or intermittent limit	Angle control retained inside the allowed travel	Torque vectoring and reference adaptation; required curvature and rate [21,22]
Actuator bias	Constant, progressive drift, or intermittent	Offset between requested and delivered steering input	Bias estimation and compensation; residual separation and detection delay [23]
Road-wheel/actuator feedback fault	Constant bias, drift, intermittent corruption, or loss	Actuation remains available but feedback is corrupted	Signal reconstruction and fault isolation; distinguish sensor corruption from mechanical failure [24–26]
Active erroneous steering	Progressive runaway, oscillatory, or intermittent	Unintended torque or angle output continues before successful isolation	Bound the active disturbance and isolate the channel; then identify the actual retained mechanical state [1,16]
Handwheel feedback actuator fault	Abrupt, progressive, or intermittent	Feedback torque is lost or corrupted, or the handwheel jams; road-wheel actuation may remain intact	Use an independent demand/authority path if available; include the altered driver interaction [2,5]
Driver-input sensor fault	Constant bias, progressive drift, intermittent signal, or sustained loss	Incorrect or unavailable driver demand; road-wheel actuator can remain healthy	Validate or reconstruct the intended demand; do not equate input loss with road-wheel torque loss [2,5]
Controller or communication loss	Abrupt loss, intermittent dropout, or persistent stale output	Held command, torque-off state, or active erroneous output, depending on architecture	Account for timeout and isolation behavior; use the resulting measured wheel state and activation delay [1,2,5]

Angle saturation is a different condition. Within the available travel, the steering response may remain accurate. Outside that travel, additional demand cannot be realized. Static output-feedback control has been studied with both steering gain faults and angle saturation, using torque vectoring to support path tracking [21]. This distinction matters during recovery: a small-angle lane-holding task may remain feasible after a travel restriction, while an avoidance maneuver may not. The fault severity is task-dependent even if the actuator limit is constant.

A locked-angle fault fixes the orientation of a wheel or axle. A nonzero lock angle creates a persistent lateral-force tendency that the healthy actuators must counter. Dynamic model reconstruction has been used to represent steering locking in four-wheel-steering vehicles [19]. The failed wheel's actual angle, axle location, and load determine this distur-

bance and the resulting difference between left- and right-turn capability. Retaining these quantities in the reconstructed model preserves the force imbalance that drives recovery.

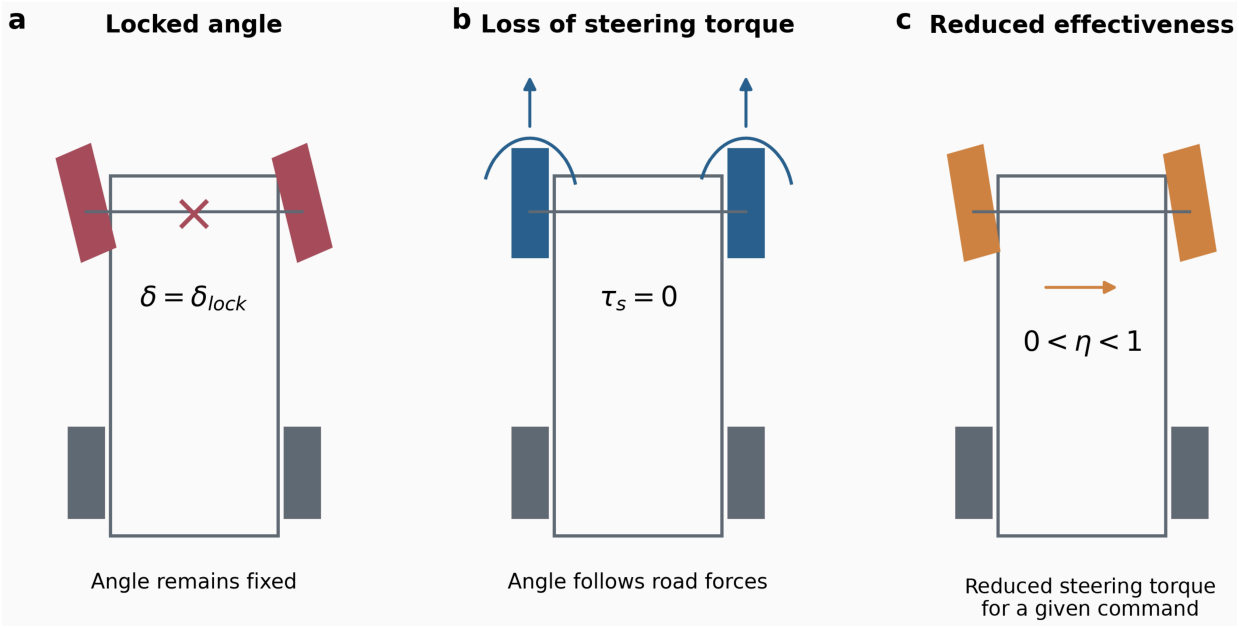


Figure 1. Mechanical steering states after failure. (**a**) Locked angle. (**b**) Loss of steering torque. (**c**) Reduced effectiveness. δ, road-wheel angle; τ_s, steering torque; η, effectiveness factor.

Loss of steering torque leaves a mechanical subsystem that can move under aligning moments and forces acting through the steering geometry. Its response depends on rack inertia, damping, steering ratio, friction, and longitudinal-force moment arms. Differential brake-actuated steering uses this interaction as a source of redundancy [20]. The induced wheel motion can reinforce or oppose the direct body yaw response, so prediction requires both the applied yaw moment and the lateral force generated by the changing wheel angle.

A measurement fault preserves physical actuation but corrupts the feedback used to control it. An angle bias can produce a persistent true-angle error. Resolver faults affect reconstructed rack force [28], while extended Kalman filtering can compensate wheel-angle sensor faults [24]. Correctly separating these faults from actuator failure allows the controller to retain usable steering. An unnecessary switch to differential steering instead consumes tire force and can cause deceleration.

Active erroneous steering requires a different model from torque loss. A runaway or oscillating actuator continues to apply unwanted effort until isolation succeeds. Recovery prediction must include that effort and any resulting wheel motion. Only after isolation can the controller use the measured retained state, such as a held angle, free response, or residual resisting torque. Table 2 therefore separates bounded actuator bias from uncontrolled active output [1,16].

Handwheel feedback and driver-input sensing lie upstream of road-wheel recovery [2,5]. A failed feedback motor can distort steering feel while road-wheel actuation remains available. A corrupted input sensor can instead create an incorrect road-wheel demand. Controller or communication loss may freeze a command, remove torque, or leave active erroneous output, depending on watchdog and power-stage behavior. These faults are retained in the taxonomy; the subsequent motion analysis uses their observed road-wheel state rather than assigning every communication loss to free steering.

2.2. Homogeneous and Heterogeneous Redundancy

Homogeneous redundancy supplies another actuator of the same type. Dual motors, multiple windings, independent inverters, and duplicated sensing can preserve the steering path after an electrical failure. The architecture depends on independence across sensing, computation, power, and mechanics [29,30]. A shared rack jam or power-supply failure can disable both motor paths. During healthy operation, unequal motor torque can also create internal loads, oscillation, and wear. Coupled control and disturbance rejection address synchronization [31–33], while multi-phase machines accommodate selected electrical faults within the motor [34,35]. These approaches retain angle control when the mechanical path remains usable. The surviving motor or winding's continuous current and transient torque limits set the available reserve.

Heterogeneous redundancy produces recovery forces through a different actuator type. Rear steering, differential traction, and differential braking replace selected effects of front steering. Figure 2 contrasts dual-motor redundancy with differential-steering geometry. The former preserves the original actuation path; the latter uses longitudinal wheel forces to generate steering or yaw action. Their response times, energy requirements, and tire-force demands follow from these different physical routes.

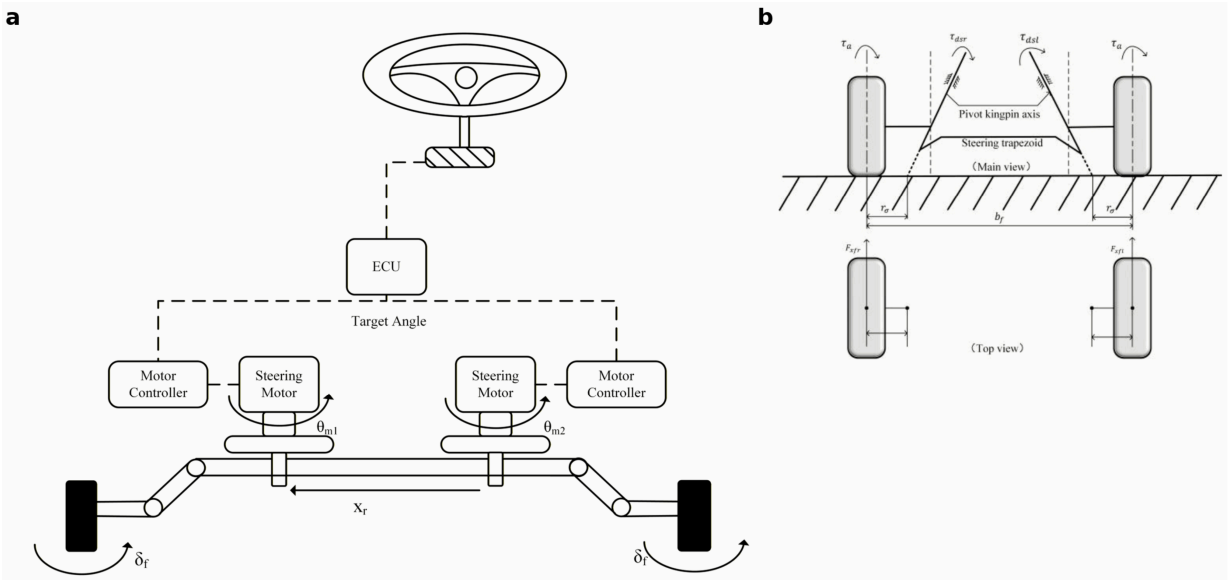


Figure 2. Steering redundancy mechanisms. (**a**) Dual-motor steer-by-wire architecture. (**b**) Differential-steering geometry. Reproduced from Figure 1 of Liu et al. [36], and reproduced from Figure 4 of Han et al. [37], respectively, under CC BY 4.0.

Torque vectoring changes the left–right longitudinal-force difference to generate a yaw moment about the vehicle center of mass. Backup-steering studies demonstrate its use with restricted front steering [38]. The lateral response develops through tire slip and body rotation. Near the friction limit, longitudinal force used for yaw control reduces the lateral reserve at the same wheel. Usable corrective yaw moment therefore depends on combined tire demand as well as available motor torque.

Differential steering uses longitudinal force to move the steering mechanism itself [39–41]. Its steering-axis moment differs from the body yaw moment produced by the same force. Dominguez-Garcia et al. [9] modeled selective braking with the primary steering actuator disconnected. Römer et al. [42] distinguish the force lever arms of wheel-hub drives and shaft-driven wheels. This distinction matters when braking and traction are assigned interchangeably in a recovery allocator.

Figure 3 defines the geometry for a straight left wheel with zero caster and camber. The vehicle axes are x forward, y left, and z upward. The unit steering-axis vector e_k points upward, so $e_{kz} > 0$; positive steering torque acts about e_k by the right-hand rule. G is the steering-axis intersection with the ground, P the contact point, C the wheel center, and A the steering-axis point at wheel-center height. Define the signed offsets $s_g = y_P - y_G$ and $s_c = y_C - y_A$. With wheel radius R, the geometry gives

$$s_c = s_g - R\frac{e_{ky}}{e_{kz}}$$

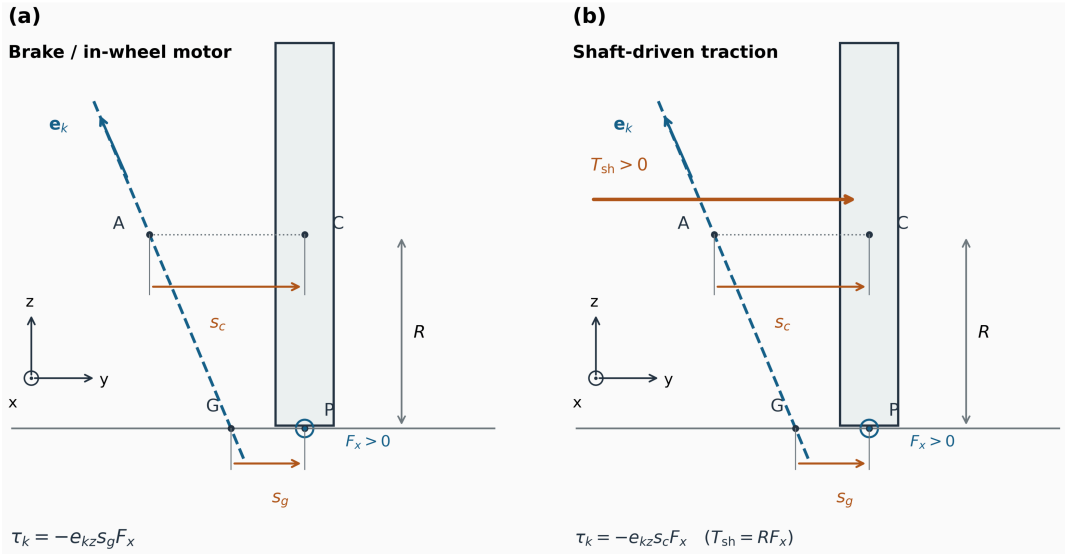


Figure 3. Signed steering geometry for a straight left wheel, viewed from the front. (**a**) Brake or in-wheel motor. (**b**) Shaft-driven traction. G, ground intersection of the steering axis; P, contact point; C, wheel center; A, steering-axis point at wheel-center height. The circled dot denotes +x toward the viewer. Offsets are positive along +y; e_k points upward. Zero caster and camber are assumed.

Consider the wheel and knuckle as one assembly. For the longitudinal-force contribution, the contact force acts at P and an external half-shaft torque T_{sh} acts about +y. Projecting their moment about G onto the steering axis gives

$$\tau_k = e_k \cdot \left[(r_P - r_G) \times (F_x e_x) + T_{sh} e_y \right]$$

$$\tau_k = -e_{kz} s_g F_x + e_{ky} T_{sh}$$

A conventional wheel brake reacts through its caliper on the knuckle; an in-wheel motor reacts through its stator on the same assembly. Their drive or brake torque is internal to this free body, so $T_{sh} = 0$ and the longitudinal-force moment is $-e_{kz} s_g F_x$. A chassis-mounted motor supplies an external shaft torque. Under quasi-static wheel rotation, $T_{sh} = RF_x$, giving

$$\tau_k = -e_{kz}\left(s_g - R\frac{e_{ky}}{e_{kz}}\right)F_x = -e_{kz} s_c F_x$$

Thus, brake and in-wheel-motor forces use the ground-level scrub offset, whereas shaft-driven traction uses the wheel-center offset [42]. For the left wheel shown, positive s_g and braking force $F_x < 0$ produce positive steering torque; reversing s_g reverses that effect. The right wheel uses the mirrored geometry with the same vehicle-frame signs. The derivation neglects wheel rotational acceleration and joint moments. Caster, camber, tire-aligning moments, and steering resistance require the corresponding full moment balance. Negative-offset braking can consequently oppose the intended steering response even when its direct body yaw moment has the desired sign [13].

Rear-wheel steering creates lateral force without requiring the same left–right longitudinal-force difference. It can therefore preserve tire resources that differential braking would use. Rear-steering fault recovery and nominal path-following studies provide the basis for this substitution [43,44]. Its contribution changes with speed and with the condition of the front wheels. A rear angle that compensates a locked front axle need not compensate an unpowered front axle that moves in response. The rear-steering range and rate must also be considered together: a sufficient final angle can arrive too slowly to prevent the initial departure.

2.3. Fault Combinations and Mechanical Coupling

Steering recovery also depends on the health of the substitute actuators. An unavailable wheel motor can remove the force needed for one yaw direction. Multiple-motor fault studies describe how wheel-torque distribution changes with actuator availability [45,46]. Their drive-system constraints define which wheel-force combinations remain available for steering substitution. The resulting capability can be asymmetric even when several motors remain healthy.

Mechanical coupling can also create faults that do not align with the controller's channel structure. A shared rack couples left and right road-wheel angles. Independent corner modules remove that rack but introduce separate toe-angle and synchronization concerns. Dynamic toe variations have been examined in four-wheel independent steering [47]. After one corner locks, the healthy corner on the same axle may generate substantial tire scrub if commanded according to a nominal common-angle model. The control allocation should retain individual wheel orientation and loading when this asymmetry is material.

We propose that the steering-to-vehicle interface reports the retained mode (controlled angle, controlled torque, or passive response), measured wheel angle, admissible torque and rate bounds, and the time to activate a new command. This extends the actuator-state information used in demonstrated allocation [48] and the degraded constraints used in velocity adaptation [22].

3. Residual Actuation Capability and Recoverable Motion

The force balances and feasible-set definitions below provide the analytical basis for comparing the cited controllers.

3.1. From Individual Wheel Limits to Vehicle Forces

The remaining control capability can be described first in force space. Let the commanded vehicle action be a longitudinal force, a lateral force, and a yaw moment. Each wheel contributes through its force direction and its position relative to the center of mass. For fixed wheel angles, this mapping is linear in the wheel-force components. The admissible components are bounded by tire loading, friction, motor torque, brake torque, and steering condition. A fault changes those bounds and sometimes changes the mapping itself. Force-domain analysis and capability-based control use this description to connect actuator availability to vehicle behavior [49,50].

A right-handed vehicle frame is used throughout: x points forward, y to the left, and z upward. Positive yaw rate r and yaw moment M_z turn the vehicle to the left. The position of wheel i is (x_i, y_i), measured from the center of mass. Its longitudinal and lateral tire forces are F_{xi} and F_{yi}. Positive longitudinal force is traction and negative longitudinal force is braking. Neglecting aerodynamic and road-grade forces, the planar balances are

$$m(\dot{v}_x - r v_y) = \sum_i F_{xi}$$

$$m(\dot{v}_x + rv_y) = \sum_i F_{xi}$$
$$I_z\dot{r} = \sum_i (x_i F_{yi} - y_i F_{xi}) \quad (1)$$

Here, m is vehicle mass, I_z is yaw inertia, v_x and v_y are body velocities, and r is yaw rate. Different force distributions can produce the same yaw moment while changing longitudinal acceleration and lateral force. A braking-dominated solution changes speed; a steering-dominated solution changes the balance of front and rear lateral forces. Their subsequent trajectories can differ even when the initial yaw response matches.

For straight wheels with left and right force resultants at $y = +b/2$ and $y = -b/2$, respectively, b denotes track width. Their longitudinal-force contribution is

$$F_X = F_L + F_R, \quad M_z = \frac{b}{2}(F_R - F_L) \quad (2)$$

F_L and F_R are the total longitudinal forces on the left and right sides. Thus, $F_R > F_L$ produces a positive left-turn yaw moment. Equal symmetric bounds F^- produce a diamond-shaped feasible domain in the F_X–M_z plane: increasing net traction reduces the available left–right force difference. Restricting the right-side positive bound to $0.35F^-$ makes the domain asymmetric. Braking-only operation confines both side forces to the interval from $-F^-$ to zero. Figure 4 shows these normalized analytical cases. Traction and yaw demands that are individually feasible can exceed the shared force limits when requested together.

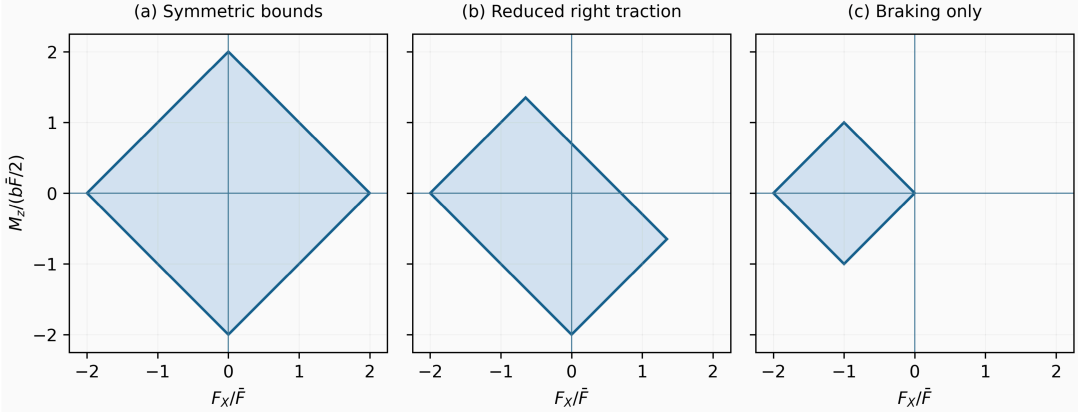


Figure 4. Normalized longitudinal-force and yaw-moment domains. (**a**) Symmetric side-force bounds. (**b**) Right-side positive bound reduced to $0.35F^-$. (**c**) Braking-only bounds. F^- is the reference side force, and b is track width. These static amplitude envelopes use fixed geometry and exclude actuator-rate and delay constraints.

Axle loading, load transfer, and unequal drive and brake capacities reshape this domain in a real vehicle. Motor limits change with speed, temperature, and supply conditions. Tire forces change with slip and wheel angle. Updating the admissible set with these states allows the allocator to represent the corrective force available during recovery. A yaw-moment bound based on nominal motor torque alone omits the changing tire and actuator constraints.

An inverter current limit restricts torque at each wheel, while the available DC voltage further restricts torque as motor speed rises [51]. Battery charge and discharge power limits depend on state of charge (SOC), temperature, and pulse duration [52]. Low SOC can reduce propulsion reserve, while high SOC or a cold battery can curtail regenerative braking [52,53]. Drives sharing one battery are also coupled by the pack power limit. Their individual peak torque ratings cannot be requested simultaneously if the combined DC demand exceeds that limit.

For steering substitution, these constraints reduce the left–right torque difference available for body yaw control and, where the geometry permits, steering-axis actuation. Reduced regeneration removes part of the negative motor-torque reserve; discharge or inverter-current limits restrict the positive reserve. Friction brakes can replace unavailable regenerative torque within their own magnitude, rate, and thermal limits [53]. They still share the tire-force budget with lateral control. The allocator therefore needs separate driving and regenerative torque bounds, friction-brake bounds, and a shared battery-power constraint. Updating these bounds with the electrical and thermal state prevents the recovery controller from requesting a yaw moment that the powertrain cannot deliver.

The tire constraint is particularly important during simultaneous cornering and speed reduction. A friction ellipse is often used to limit combined longitudinal and lateral demand. Its axes should correspond to a consistent tire model and normal load. Where lateral force is already large, increasing braking or traction can reduce the available lateral reserve. Force-allocation research on split-friction surfaces and actuator faults addresses this interaction directly [54]. Wheel-specific friction and normal-load estimates describe the changing force reserve during recovery.

3.2. Static Capability and Capability over Time

A static force region is an amplitude envelope at a specified vehicle state and steering geometry. It answers which force combinations satisfy the settled actuator and tire limits. Figure 4 depicts this type of envelope; it contains no steering-rate, brake-build-up, motor-response, or diagnosis-delay constraint. Membership in a static region therefore does not show that a corrective force can arrive before the vehicle reaches a road boundary.

A dynamically reachable force region additionally starts from the current actuator states and evolves over a stated time horizon. For a rate-limited actuator, its change over the available response time cannot exceed its rate bound multiplied by that time; a command-transfer delay reduces the available interval. The force mapping must also evolve with wheel angle, tire slip, and normal load. With the vehicle state held fixed, these rate and delay restrictions reduce the static envelope to a reachable subset. With changing vehicle states, the dynamic region must instead be compared with the corresponding sequence of static envelopes. A final rear-steering angle inside its travel limit can thus be feasible statically and unavailable during the initial correction.

Adaptive predictive control can update its model using steering-sensitivity estimates [55]. Reconfigurable model predictive control (MPC) updates both the model and the post-fault constraints [56]. These changes affect predicted forces and the time required to produce them. Model reconstruction and actuator-rate updates therefore work together: the former describes the degraded response, and the latter constrains the transition to the requested action.

The mechanical fault changes this time evolution. After torque loss, an initially retained front-wheel angle can move under road forces and create an adverse transient before differential steering develops. A locked wheel retains its angle, but its lateral force still changes with slip and speed. Direct yaw action from differential wheel force and the later lateral-force response from wheel rotation must therefore remain separate in the prediction model [13,20]. Similar settled force limits can conceal different recovery transients.

The force-to-steering mapping must use the actuation-specific lever arms defined in Section 2.2. Longitudinal force contributes through the ground-level offset for braking and wheel-hub drive, or through the wheel-center offset for shaft-driven traction [42]. Lateral tire forces and pneumatic trail add aligning moments. Inertia, friction, damping, and compliance then determine how the resulting torque changes the wheel angle [13,20]. A larger wheel-force difference therefore changes both body yaw and the transient steering response.

3.3. Force Authority and Task Feasibility

Rank and singular values describe the local directions in which an actuation mapping can produce forces. Force-domain analysis uses these measures to compare drive and steering fault combinations [49]. Forces and moments require stated normalization because they have different units. Full rank identifies available directions, while actuator bounds determine the magnitude available in each direction. Feasibility asks whether admissible inputs can produce the requested force or state transition. Task completion adds road boundaries, obstacles, timing, and a terminal condition. These criteria explain why yaw stabilization and corridor-contained lane changing can require different recovery actions. A vehicle may retain sufficient authority to bound yaw and sideslip yet need a lower speed to complete the maneuver within the road.

The recovery horizon begins when reconfigured commands become active, at t_c. Before that time, the commands are inherited from the pre-transfer controller and cannot be chosen freely by the recovery optimizer. The initial recovery state is predicted by propagating the estimated state at recognition time t_d through the degraded dynamics and inherited commands until t_c. The subsequent trajectory must remain within the road corridor and reach a terminal set for stable continuation or standstill:

$$u(t) \in U_f(x,t), \quad x(t) \in X_{\text{safe}}$$
$$x(t_c + T) \in X_{\text{terminal}}, \quad t \in [t_c, t_c + T] \tag{3}$$

Here, t_d is the fault-recognition time, t_c is the command-reconfiguration time, and T is the horizon measured from t_c. The same corridor constraint is checked over the predicted transfer interval $[t_d, t_c]$, using the inherited commands. The state at t_d includes motion accumulated during diagnosis. X_{safe} constrains the vehicle footprint and relevant motion states; X_{terminal} defines completion. Track width is denoted by b, leaving t exclusively for time.

Velocity adaptation provides a direct means of enlarging the set of feasible paths. Lower speed usually reduces the lateral acceleration required for a given curvature, but the transition to that speed also consumes distance and tire force. Unified fault-tolerant control with adaptive velocity planning explicitly connects these decisions [22]. Trajectory reshaping based on a fault-tolerant feasible region extends the connection to the desired motion itself [57]. These studies support treating the speed and path as adjustable control objectives when the original reference lies outside the degraded envelope.

Table 3 compares recovery mechanisms and the capability represented after failure. Figure 5 shows how two published architectures connect motion demand to alternative wheel actuation. Their upper controllers generate vehicle-level requests, and their lower stages translate these requests into commands under the stated fault models.

Table 3. Representative formulations of residual actuation and motion recovery.

Study	Recovery Mechanism	Capability Represented	Evaluation Focus
Kirli et al. [38]	Torque vectoring	Backup yaw action after steering loss	Vehicle response with alternative actuation
Stolte et al. [58]	Nonlinear predictive reconfiguration	Updated model, weights, and constraints	Fault-conditioned vehicle motion
Seiffer et al. [48]	Differential steering allocation	Coupled longitudinal forces and steering action	Force-to-steering conversion
Koysuren and Cakmakci [56]	Reconfigurable MPC	Degraded actuation model and constraints	Coordinated predictive response

Table 3. *Cont.*

Study	Recovery Mechanism	Capability Represented	Evaluation Focus
Wang et al. [50]	Capability-based fault tolerance	Remaining actuator capability	Control matched to residual authority
Ha et al. [13]	Differential braking	Kingpin offset and braking constraints	Vehicle-anchored model; geometric parameter sweep
Ha et al. [12]	Rear steering and torque vectoring	Locked angle versus loss of steering torque	Comparative vehicle experiments
Lu et al. [49]	Force-domain analysis	256 drive and steering fault configurations	Attainable forces and singular-value measures
Shi et al. [57]	Reference reshaping	Fault-tolerant feasible region	Adaptation of the motion demand
Qi et al. [59]	Differential steering and yaw control	Steering failure with roll dynamics	Co-simulation and hardware in the loop

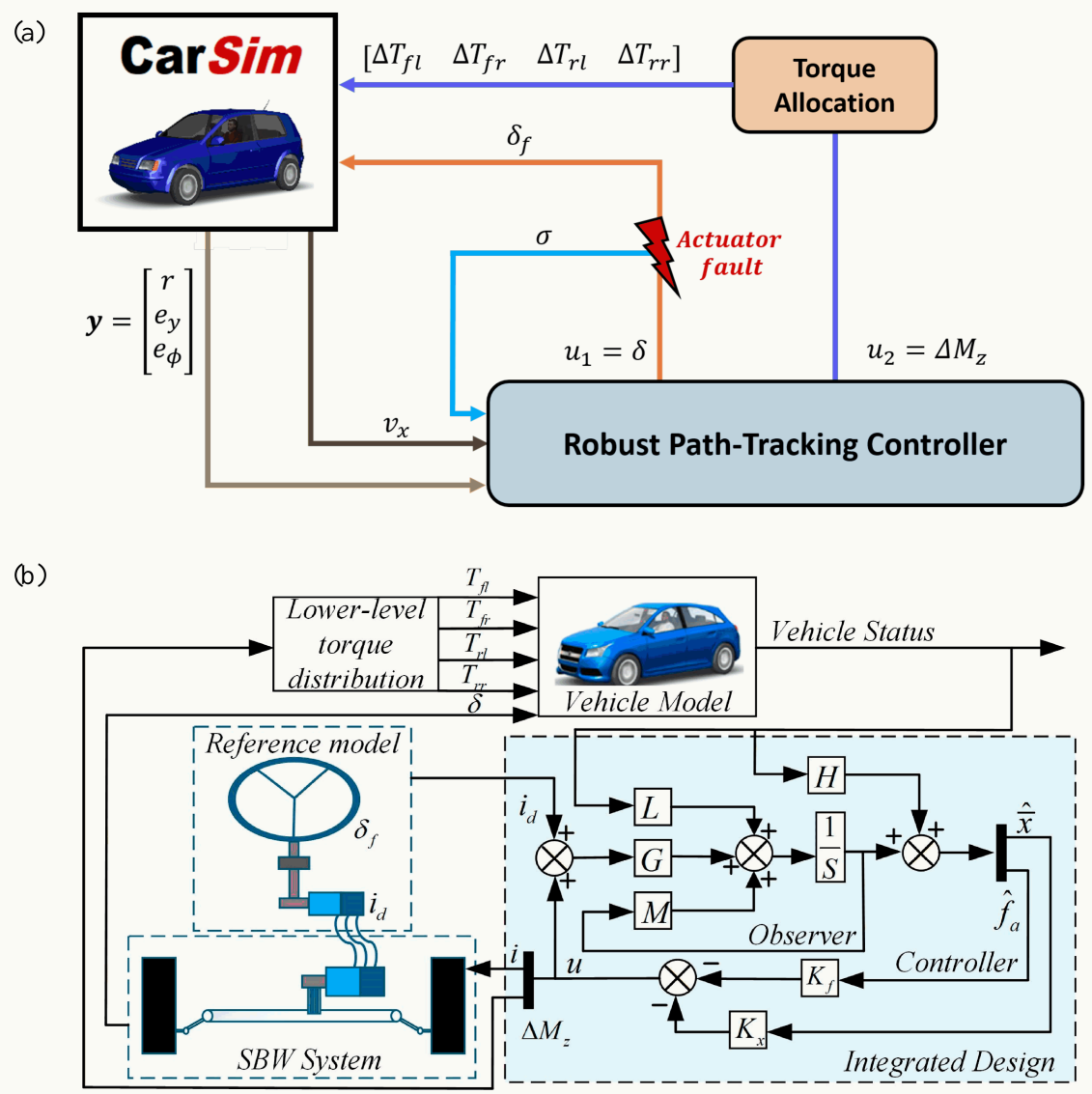


Figure 5. Control architectures for steering-fault accommodation. (**a**) Static output-feedback control with torque vectoring. (**b**) Integrated fault estimation and fault-tolerant control. Reproduced from Figure 3 of Meléndez-Useros et al. [21], and reproduced from Figure 3 of Wang et al. [60], respectively, under CC BY 4.0.

4. Fault Diagnosis and the Transition to Recovery

4.1. Estimating the Fault State That the Controller Needs

Fault detection identifies abnormal behavior, isolation locates the affected channel, and estimation reconstructs fault magnitude or a physical parameter. Recovery uses these outputs to select admissible commands. Reduced effectiveness, measurement bias, saturation, lock, and loss of steering torque call for different actions. Distinguishing these states determines whether the controller can retain the steering motor, compensate for its input, or transfer control to other actuators.

Observers connect actuator behavior with measured vehicle motion. A steering model predicts angle or rack motion from motor input, while a vehicle model predicts yaw and lateral response from wheel angles. Residuals locate disagreement within this chain. Adaptive output feedback has been developed for interconnected vehicle dynamics with unknown actuator faults [61]. Integrated observer and controller synthesis incorporates estimation error directly into steering-fault control [60]. Fault identification also depends on separating effects that produce similar residuals. Sensor bias, actuator bias, tire-stiffness changes, road bank, and crosswind can all alter the steering-to-yaw relation. Augmented models and separate observer channels address simultaneous actuator and sensor faults [25,62]. A recent predictive scheme estimates steering-motor and angle-sensor faults before compensation [26]. These formulations use measurements of both actuation and vehicle motion to distinguish the underlying causes.

Straight driving with small steering input provides little excitation for estimating steering effectiveness. A bounded estimate available early can be more useful for recovery than a precise estimate obtained after substantial departure. Diagnostic evaluation should therefore connect fault-estimation error and delay to the commands selected and the resulting vehicle motion.

Fault classification also changes the plant used for recovery. Mistaking a free mechanism for a locked one gives an incorrect wheel-angle prediction; mistaking a sensor bias for torque loss can discard usable actuation. Kim and Kim [23] test bias reconstruction and compensation, while the complete-failure comparisons distinguish fixed-angle and torque-loss dynamics [12]. These are different diagnostic tasks, even when both are called steering-fault accommodation.

4.2. Observer and Learning Methods

Extended Kalman filtering reconstructs wheel-angle measurements, while multiple-model adaptive filtering addresses different sensor-failure patterns [24,63]. Explicit process and measurement-noise models support residual interpretation. Fault isolation depends on how well the model separates corrupted sensing from physical steering disturbances. The relevant outputs are reconstructed angle, residual behavior, and the inferred fault state.

Sliding-mode observers reconstruct unknown inputs through their error dynamics. Kim and Kim [23] evaluated constant, drifting, and intermittent steering biases using an adaptive observer. Figure 6 reproduces the compensation architecture and the heading-angle RMS comparison for the constant actuator-bias scenario only. The two plots cover the full maneuver and the fault-active interval; they do not combine the three temporal fault patterns.

Learning methods broaden the patterns that can be recognized from measured signals. A bidirectional long short-term memory (Bi-LSTM) model combined with a sequential probability ratio test has been studied for steering fault detection and tolerance [64]. Finite-state and extreme-learning-machine methods have addressed diagnosis and prognosis [65]. More recent work combines learned sensor-fault detection with robust actuator-fault estimation [66]. These models infer fault patterns from signal history. Comparing the inferred

state with the measured mechanical response connects their output to the actuation used for recovery.

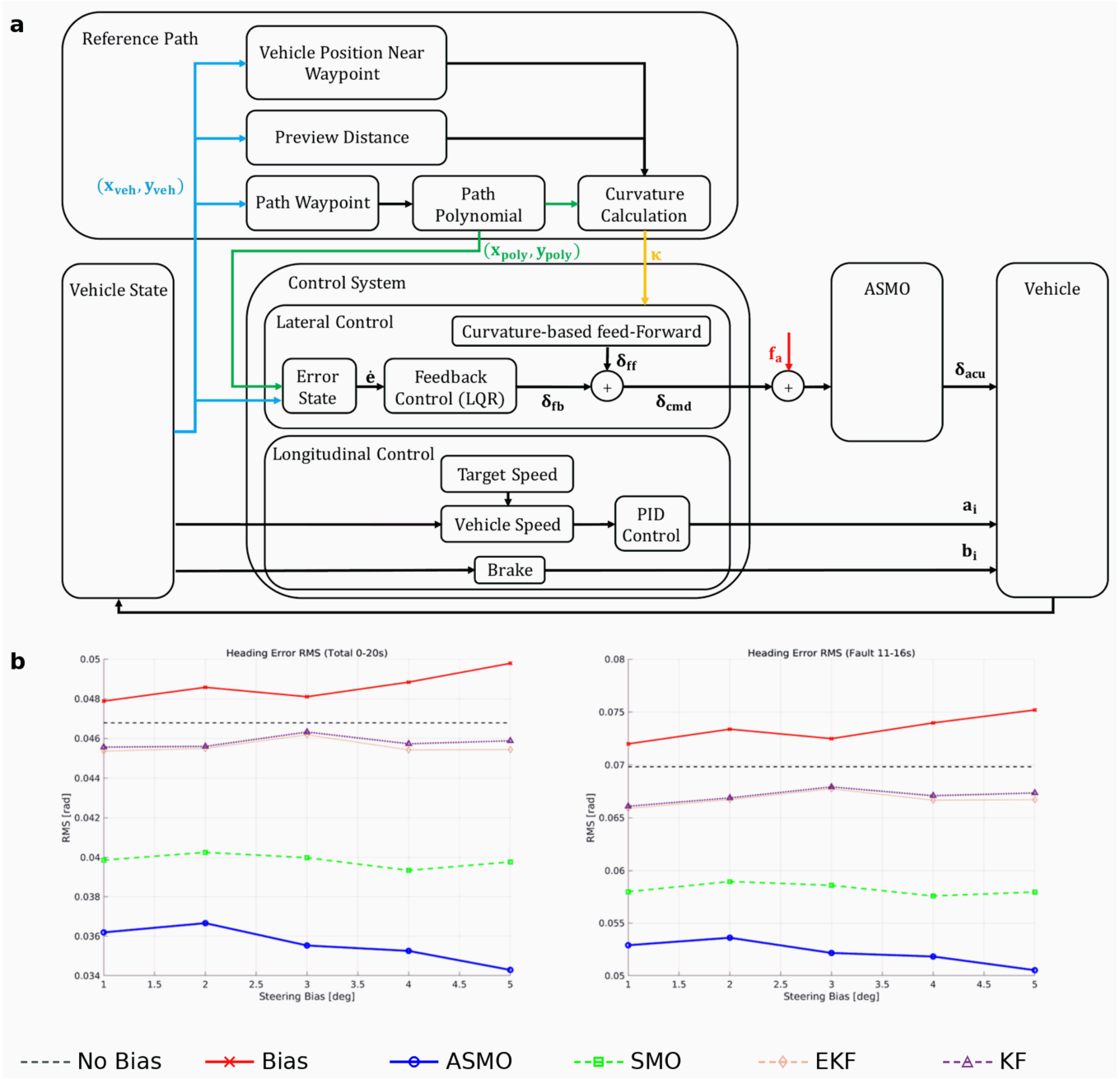


Figure 6. Observer-based steering-bias compensation. (**a**) Control architecture. (**b**) Heading-angle RMS error for the constant actuator-bias scenario, evaluated over the full maneuver (0–20 s) and the fault-active interval (11–16 s). The block diagram and plots are reproduced from Figures 1 and 14c,d, of Kim and Kim [23], under CC BY 4.0.

Training coverage determines which faults a learned diagnostic model can separate. Bias magnitude, jammed motion, and power-stage failure imply different recovery actions, so evaluation needs both in-category faults and unfamiliar fault patterns. Changes in load, road condition, and combined sensor-actuator faults test the stability of those decisions. Reporting uncertainty alongside the selected actuation mode links classification performance to available recovery commands.

Gaussian-process methods relate measured behavior to fault estimates and predictive uncertainty [67]. That uncertainty is conditional on the represented fault mechanisms and operating data. Learning-based tracking and stochastic predictive control also link estimation to corrective action [68,69]. Their use in recovery depends on how those model assumptions translate into admissible steering and wheel-force commands.

Experimental sensor-fault estimation with nonlinear tire models tests residual behavior beyond simple lateral-model assumptions [70]. Healthy high-slip maneuvers, uneven loading, and steering reversals provide relevant baselines for steering diagnostics. Comparing their residuals with faulted runs reveals whether a mode switch follows a fault or an ordinary vehicle disturbance. Table 4 summarizes the diagnostic methods and the information they provide for motion recovery.

Table 4. Diagnostic methods and the information needed for motion recovery.

Method Family	Representative Studies	Estimated Information	Main Evaluation Variable
Kalman and multiple-model filtering	[24,63]	Wheel-angle or sensor-fault state	Bias isolation under model and noise variation
Adaptive or sliding-mode observers	[23,61]	Unknown actuator input or steering bias	Delay, noise sensitivity, and fault amplitude
Integrated estimation and control	[26,60]	Fault state used by the controller	Closed-loop response during reconstruction
Simultaneous sensor and actuator estimation	[25,62]	Distinct sensor and physical actuator faults	Identifiability with shared residuals
Sequence learning and statistical tests	[64,66]	Fault patterns from signal history	Unseen faults and changing operating conditions
Finite-state prognosis and regression	[65,67]	Degradation state or fault magnitude	Uncertainty and transfer to capability bounds
Dual-motor supervision	[71]	Motor failure and steering resistance	Isolation and healthy-motor load

4.3. Diagnosis Delay and Command Handover

The vehicle moves throughout detection and isolation. Total response delay comprises acquisition, filtering, persistence tests, communication, computation, command transfer, and actuator build-up. A fast algorithm can still respond late if its threshold rule requires sustained evidence. Figure 7 places these delays on a common timeline from fault onset through recognition and reconfiguration to settled recovery. This timing links diagnostic decisions to the motion already accumulated before correction.

ISO 26262 relates fault response to a hazard-specific fault-tolerant time interval (FTTI) [72]. In Figure 7, the interval from fault onset to recognition is the fault detection time interval. The subsequent fault reaction time interval includes command transfer and actuator response until a specified safe state or emergency operation is reached. Their sum must remain below the relevant FTTI. Command activation at t_c and settling at t_s are distinct events; the safety goal determines which state ends the fault reaction interval. The FTTI margin therefore depends on both diagnostic delay and the time needed to achieve the required vehicle response. Emergency operation also requires a bounded duration before transition to a safe state [72].

ISO 21448 addresses hazards from functional insufficiencies, including inadequate perception or performance assumptions in the recovery planner; electrical faults remain within ISO 26262 [73]. UNECE Regulation No. 79 adds failure-performance and driver-warning requirements for steering equipment within its scope [74]. These requirements connect the transition in Figure 7 to retained directional control and timely fault indication.

For Level 3–5 automated driving in light-duty vehicles, ISO 23793-1 specifies straight-stop and in-lane-stop minimal-risk maneuvers [75]. Recovery assessment should then follow the maneuver through deceleration to its terminal condition, recording corridor clearance, residual speed, and final heading. A low tracking RMS alone does not measure completion of that maneuver.

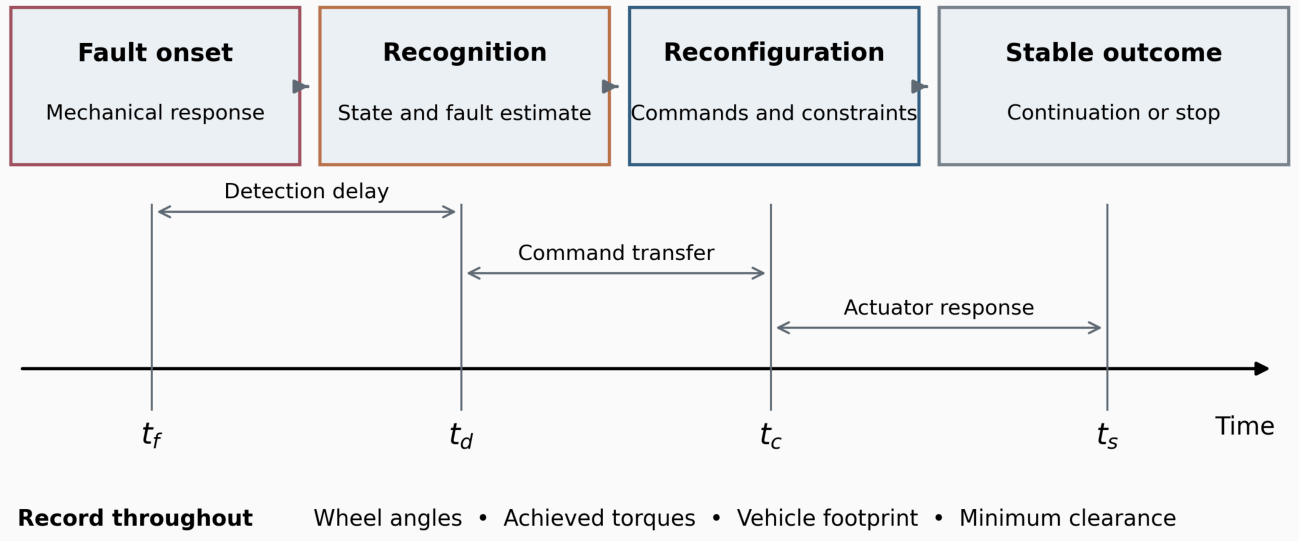


Figure 7. Recovery transition from fault onset to a settled outcome. t_f, physical fault onset; t_d, fault recognition; t_c, command reconfiguration; t_s, settled recovery.

The vehicle continues to depart during detection and transfer. A lock imposes persistent curvature, whereas torque loss can change the wheel angle throughout the interval. Heading error also accumulates into lateral displacement at a rate that increases with speed. Command transfer must account for the state reached at activation, including actuator lag and controller memory. Huang et al. [18] simulate motor-fault detection and switching; Seiffer et al. [48] test an actuator transition with externally supplied actuator-state information. The latter establishes transfer behavior without measuring an end-to-end diagnostic delay.

Communication delay changes the relation between measured and current actuator behavior. Dual-motor steering research models coupled delays and faults [18], while quantized networked control addresses restricted feedback resolution [76]. Time stamps and local supervision help separate stale information from loss of actuation. The resulting distinction determines whether recovery requires a model update, a communication response, or actuator isolation.

Intermittent faults can produce repeated transients as the controller moves between nominal and degraded modes. Degradation models and prescribed-performance methods address changing steering faults [77,78]. Entry, retention, and re-entry criteria can limit repeated switching. Re-entry requires evidence that the relevant steering capability has recovered under the current load and driving task, alongside restored sensor feedback.

5. Coordinating the Surviving Actuators

5.1. Local Compensation and Chassis Reconfiguration

Local compensation retains the steering path when the mechanism remains controllable. Increased input can offset reduced gain within surviving current and torque limits, and estimated bias can be subtracted or included in the prediction model. Robust and adaptive controllers address uncertainty in this relationship [17,79]. Mechanical freedom and continuous thermal capacity determine how much compensation can be sustained. The

local controller can communicate the resulting angle range and rate to the chassis controller as the basis for any additional actuation.

Electrical redundancy can preserve steering authority within the subsystem. Dual-redundancy control, synchronized motors, and fault-tolerant multi-phase machines provide several implementations [34,35,80]. Their available reserve depends on the failure location. An open winding, inverter fault, and stalled rotor leave different loads on the healthy actuator. A mechanically coupled failed motor may supply resisting torque, so isolation and the failed machine's passive behavior belong in the post-fault model.

Dual-motor synchronization reduces internal torque imbalance before and after fault accommodation. Liu et al. [36] report lower current mismatch and shorter settling in their modeled synchronization strategies. These electrical outcomes characterize the current and torque response available to the steering mechanism. Section 7 places this component-level evaluation alongside the vehicle and hardware-in-the-loop evidence. Chassis reconfiguration redistributes the motion task when local compensation reaches its limits. A hierarchical controller commonly requests longitudinal force and yaw moment, then allocates wheel commands within surviving actuator bounds. Han et al. [37] combined predictive trajectory control, differential-steering control, and quadratic-programming torque distribution in a steering-failure simulation. The interface between these layers links tracking demand to achievable force and provides the point at which saturation information can return to the upper controller.

Table 5 classifies controllers by their role in recovery. Passive robust control accommodates a defined fault range within one control law. Active control uses fault estimates and reconfiguration to adapt the response. Distributed control coordinates healthy steering corners while estimating unknown actuator effects [81]. Comparisons require a common physical fault model and surviving actuator bounds because gain reduction, a fixed angle, and torque loss impose different tasks.

Table 5. Control approaches classified by their role in recovery.

Approach	Primary Role	Representative Studies	Governing Constraint
Local robust or adaptive compensation	Restore steering response	[17,79,82]	Remaining torque and mechanical controllability
Motor or winding redundancy	Preserve the steering actuation path	[33–35,80]	Failed-machine resistance and shared mechanics
Hierarchical force allocation	Redistribute chassis effort	[37,48,83]	Coupled yaw, steering, and tire-force demands
Predictive reconfiguration	Anticipate constrained motion	[56,58,84]	Model update, rates, and solver timing
Robust predictive control	Contain model and fault uncertainty	[85–87]	Physical basis of the uncertainty set
Distributed or sliding-mode control	Coordinate corners or reject disturbances	[81,88,89]	Saturation, switching, and achieved inputs
Learning-assisted control	Adapt models, weights, or allocation	[69,90,91]	Fault coverage and bounded fallback action
Motion adaptation	Reduce or reshape the demand	[22,57,92]	Road corridor and terminal condition

5.2. Allocation with Coupled Steering and Wheel Forces

Control allocation converts desired vehicle action into actuator commands. A representative objective penalizes mismatch between requested and achieved generalized

force, actuator effort, and abrupt command changes. The fault-conditioned problem can be written as

$$\min_{u} \|B(x)u - g_d\|_W^2 + \|u\|_R^2 + \|u - u_{\text{prev}}\|_S^2$$
$$\text{subject to} \quad u \in U_f(x,t) \tag{4}$$

The vector u contains actuator commands, $g_d = [F_{X,d}, F_{Y,d}, M_{z,d}]^{\mathrm{T}}$. is the requested generalized force, and u_{prev} is the preceding command. $B(x)$ maps commands to generalized force at the current geometry and operating state; nonlinear formulations use the corresponding nonlinear map. W weights force mismatch; R and S weight effort and command changes. These quadratic penalties use positive-semidefinite weights with consistent scaling. U_f contains the fault-conditioned magnitude, rate, tire, and power limits.

Force and moment errors require consistent scaling before weighting. A numerical error in newtons is not directly comparable with one in newton meters. Scaling by relevant force and moment ranges makes the allocation trade-off interpretable, especially after a fault changes those ranges. Road containment and stability can be imposed as explicit constraints or given priority over efficiency and nominal speed tracking. A hierarchical or lexicographic allocator then optimizes lower-priority goals within the remaining freedom. For example, it can first reduce the unmet lateral or yaw demand and then minimize unnecessary braking. The priority follows the maneuver: limited lateral clearance favors rapid departure correction, while adequate lateral space can permit a smoother controlled deceleration. Reporting that priority explains the resulting motion more clearly than the weight values alone.

Differential steering couples body yaw with steering-axis torque. Seiffer et al. [48] allocate drive and steering torques jointly, prioritize steering when drive and steering demands conflict, and feed the torque-vectoring effect back to the upper control layers. Their demonstrator tests examine the transition after actuator failure. Coordinated differential drive-assist steering and direct yaw control address the same shared wheel-force resource [83]. A joint mapping avoids assigning that resource independently to two incompatible requests.

Brake and drive commands also differ in reversibility. A friction brake produces resisting torque, whereas an electric drive can provide positive or negative torque within operating limits. A brake-based yaw command therefore changes net longitudinal force unless another actuator compensates. That compensation may increase power demand and tire utilization on the other side. Near zero speed, motor and brake behavior changes again, and the steering-axis effect of longitudinal force may be limited by static friction. A stopping maneuver therefore requires a model that covers the changing tire and steering response near standstill.

Allocation must return a usable command within the control period. Computationally efficient nonlinear allocation addresses this burden [93], but the reviewed evidence does not establish a common implemented response to solver failure. Two events require separate reporting: a problem declared infeasible, and a deadline reached before a feasible solution is available. Solver time alone cannot identify the command delivered to the actuators.

Actuator conversion dynamics affect how an allocated command becomes tire force. During wheel acceleration, wheel torque also supplies rotational inertia. Brake pressure converts to torque through temperature-dependent friction, and the motor angle converts to road-wheel angle through compliant or backlash-prone mechanics. Feedback can compensate these effects when the plant model and measurements retain them. Allocation studies at handling limits examine related model choices [94]. Their treatment connects requested wheel action to the force actually delivered at the road.

For implementation, we recommend an explicit command-selection rule. If tracking or terminal constraints cause infeasibility, soften those constraints while retaining hard

actuator and tire limits. Apply a feasible relaxed solution when it is available before the deadline. Otherwise, apply a separately validated fallback command for the current fault and request speed or path adaptation. If a deadline is missed, apply a current feasible incumbent; if none exists, reuse the previous command only after checking it against the updated constraints. If that check fails, apply the fallback command. Zero input and the previous command are not automatically feasible after a lock or a sudden loss of authority. The issued command and active branch must be recorded alongside the optimization status.

5.3. Predictive, Robust, and Learning-Based Coordination

Predictive control combines future motion, actuator rates, and road constraints in one optimization. Integrated fault-tolerant control has been developed for independent steering, driving, and braking [84]. Nonlinear predictive methods reconfigure models, weights, and constraints for over-actuated vehicles [58]. These formulations anticipate how actuator actions interact over the recovery horizon. Their implementation couples a degraded-vehicle model with a solver that updates the command within each control period, including the abrupt constraint changes at fault isolation.

Robust predictive methods represent mismatch between the model and the degraded vehicle. Tube-based path-following and cooperative actuator-fault control provide examples [85,86]. The uncertainty set covers specified steering, tire, and actuator errors and determines how much motion remains feasible. Enlarging the set reduces usable tracking authority; narrowing it increases reliance on model accuracy. Testing against the measured error range connects this trade-off to the fault transition.

Linear parameter-varying (LPV) methods offer a different balance between model coverage and computational cost. Scheduling with speed or tire properties can retain a tractable design while accounting for important operating changes. Static output-feedback steering-fault control uses measured signals without adding a full state observer [21]. LPV predictive control with direct yaw compensation has also been studied for steering failures [95]. These approaches are valuable when their scheduling variables remain reliable after the fault. A corrupted speed or steering signal can otherwise affect both the feedback and the controller selected from the schedule.

Sliding-mode and terminal-control methods address robust tracking with relatively compact implementations. Vehicle studies use adaptive terminal and super-twisting laws for degraded actuation [88,96]. Xu et al. [89] combined a fixed-time approach with differential steering, an observer, and switching, and evaluated it in simulation and hardware in the loop. The stated convergence result applies under the model and admissible-input conditions used in its derivation. Tracking errors and achieved actuator commands together show whether saturation or rate limits become active during recovery. Figure 8 presents published examples of these actuator responses.

Learning can support fault-tolerant control by estimating uncertainty, adapting a model, selecting weights, or distributing torque. Reinforcement-learning-based steering tracking and predictive torque distribution have both been investigated [90,91]. Learning an allocation policy within a physically bounded action space can reduce online effort, but the policy still needs to handle a changed number of available actuators and an asymmetric feasible set. A policy trained mainly under nominal symmetry may select a torque pair that becomes impossible after one motor is isolated.

A comparison with and without the learned component can isolate its effect on estimation or allocation when the plant, fault timing, and actuator bounds are held constant. Motor demagnetization studies address a related reduction in wheel-torque reserve [97]. Their relevance here is the remaining drive capability supplied to the steering-recovery controller.

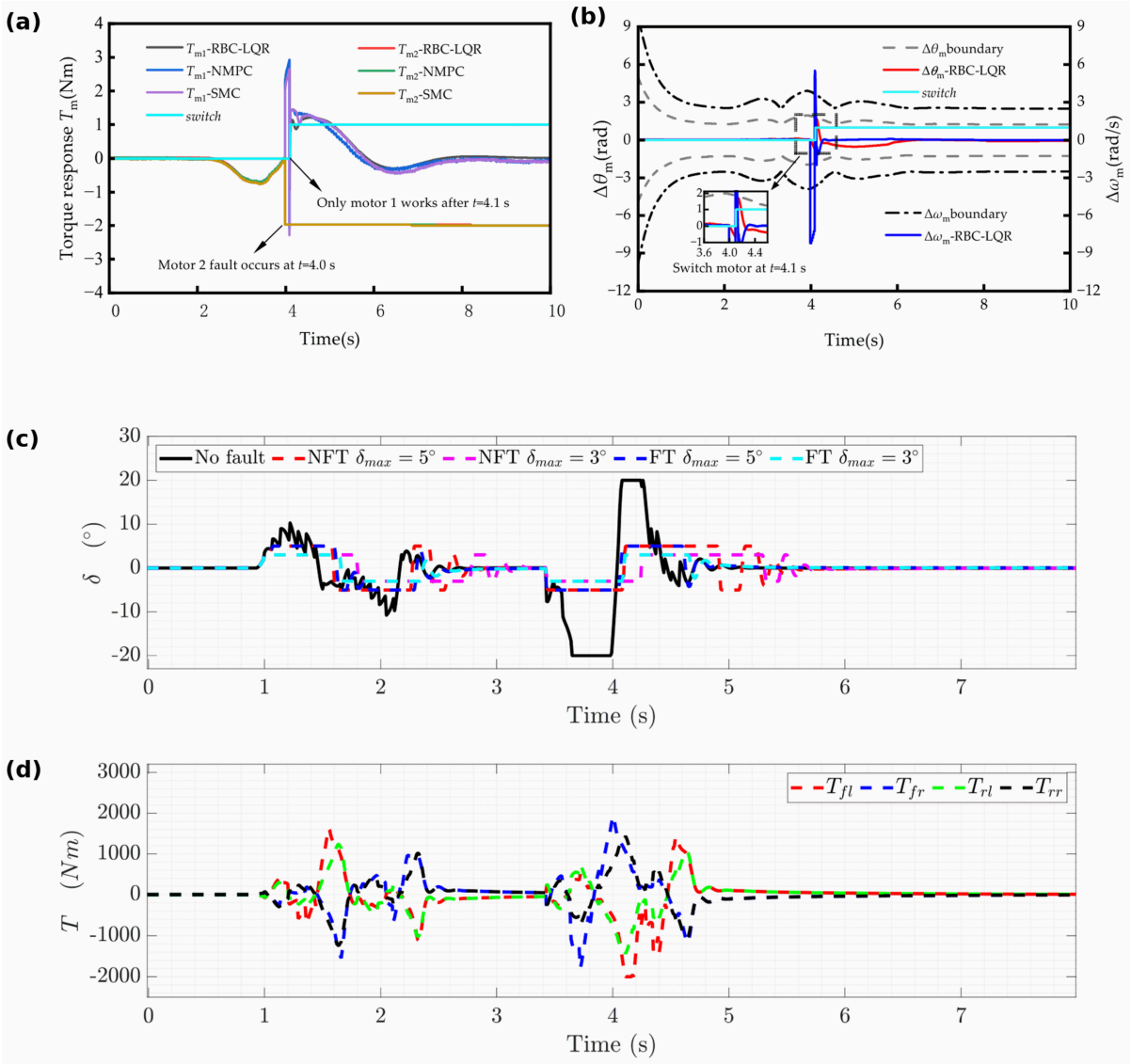


Figure 8. Actuator responses under faults. (**a**) Motor torques and (**b**) synchronization errors (reproduced from Figure 7 of Huang et al. [18]). (**c**) Steering angle and (**d**) wheel torques under angle saturation (reproduced from Figure 10 of Meléndez-Useros et al. [21]). Reproduced under CC BY 4.0.

6. Adapting the Motion Demand After Failure

6.1. Path Tracking and Feasible Continuation

A recovery controller needs a reference compatible with the degraded vehicle. Retaining the original path provides a direct tracking objective when the maneuver remains feasible, as in failed-motor trajectory control and robust tracking under bounded steering faults [98,99]. When curvature demand exceeds the available force or steering rate, sustained tracking effort can saturate the actuators. Reference adaptation changes the speed or path to bring the motion request within the remaining capability.

Actuator reconfiguration changes which channels execute the motion request; replanning changes the request itself. Han et al. [92] study replanning with hybrid fault-tolerant control, and Shi et al. [57] use a fault-tolerant feasible region to reshape the reference. These formulations connect the reference to degraded capability. The planning state must include motion accumulated before corrective actuation begins, rather than restarting the maneuver at the state of fault onset.

The terminal condition specifies the motion needed after the path correction. Stable lane following requires a suitable position and heading together with a settled yaw response. A controlled stop requires the final trajectory and wheel orientation to fit the available space, including any nonzero locked angle. Speed, position, heading, and relevant motion states therefore enter the terminal description. Road and traffic conditions determine the admissible stopping or continuation region.

Figure 9 separates two studies and their fault models. Han et al. [37] simulate differential-steering recovery after steering failure; Meléndez-Useros et al. [21] simulate path tracking with reduced steering gain. The curves illustrate tracking behavior under different operating conditions. Their quantitative results and evidence levels are compared in Table 6.

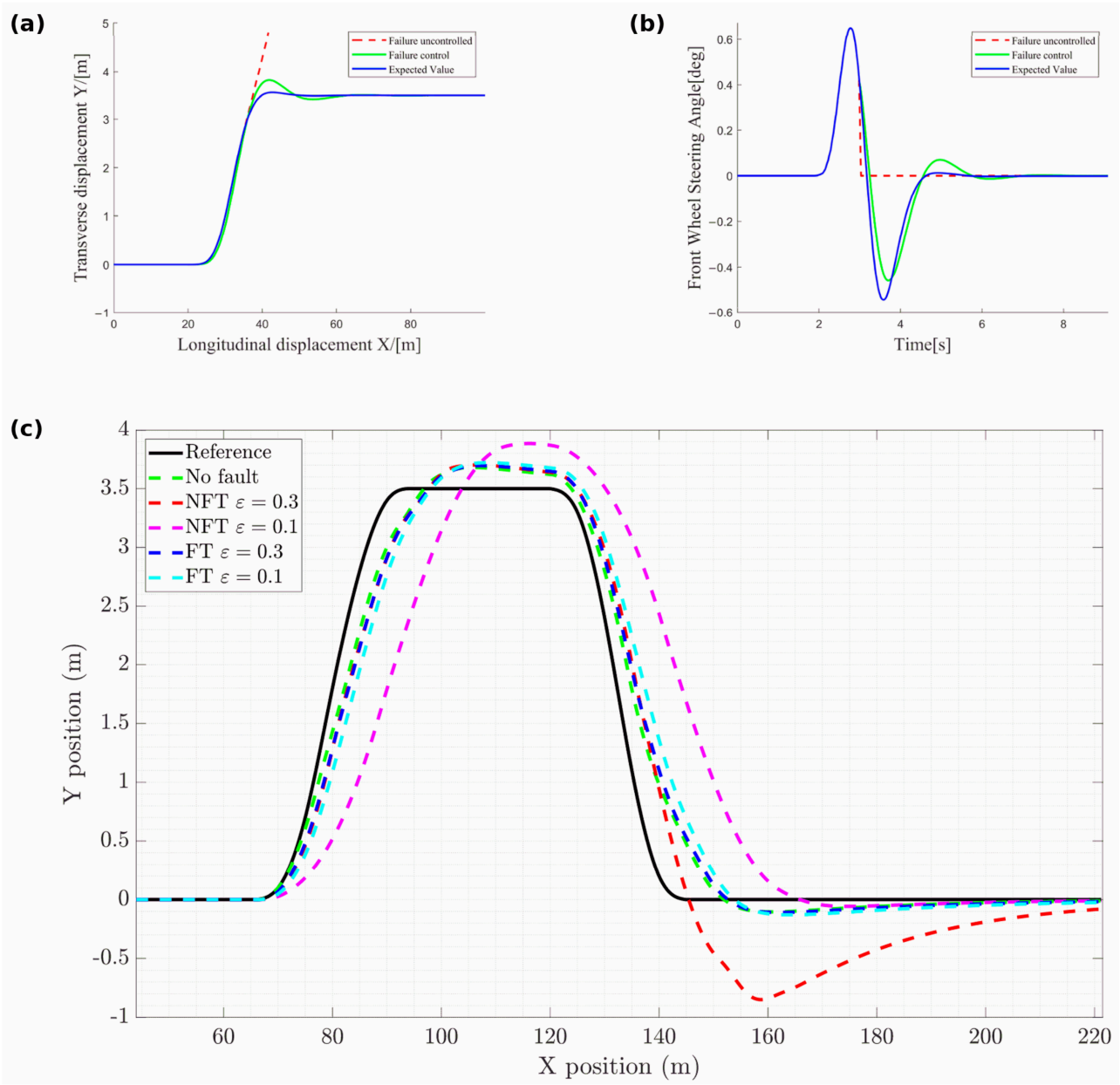


Figure 9. Tracking responses under steering faults. (**a**) Single-lane-change trajectory and (**b**) front-wheel steering angle (Reproduced from Figure 5a,b of Han et al. [37]). (**c**) Path tracking under steering gain reduction (Reproduced from Figure 7 of Meléndez-Useros et al. [21]). Reproduced under CCBY 4.0.

Table 6. Recovery results and operating conditions. NR, not reported for the selected case in the assessed source; N/A, not applicable; μ, tire–road friction coefficient. Arrows denote within-study comparisons in the stated direction.

Study/Evidence	Fault and Surviving Actuation	Maneuver, Speed, Friction; Fault Information	Reported Outcome	Vehicle-Level Interpretation
Meléndez-Useros et al. [21] Simulation	Gain loss or angle restriction; front steering and wheel-torque vectoring	Double lane change; 25 m/s; μ: NR. Fault-mode controller; diagnostic transition not evaluated.	Healthy lateral RMS/peak: 0.2497/0.7800 m. Gain 0.1: RMS 0.8071 → 0.3983 m; compensated peak 1.2064 m. 3° limit: RMS 0.6643 → 0.3519 m; compensated peak 1.0751 m.	Gain 0.3: RMS 0.4113 → 0.3030 m, but peak 0.8960 → 0.9321 m. Healthy and compensated excursions remain relevant to clearance.
Kim and Kim [23] Simulation	Constant, intermittent, or drifting bias; estimated-bias steering compensation	Double lane change; 100 km/h; nominal μ = 1.0. Separate robustness case: μ = 0.6 and mass −15%. Online observer.	Detection at 1°/5°: constant bias 606.3/76.6 ms; intermittent bias 166.8/46.6 ms; drifting bias 11,616.0/8177.1 ms. At 1° intermittent bias, lateral RMS improvement: −6.941%. Robustness comparison: lateral RMS 0.0327 → 0.0916 m and heading RMS 0.031 → 0.095 rad (nominal → perturbed).	The 1° intermittent-bias case shows slight tracking deterioration after compensation. Tracking errors also increase in the separate reduced-friction and reduced-mass robustness case.
Huang et al. [18] Simulation	Motor-2 short circuit; motor 1 retains steering	Variable-speed single lane change; 80–100 km/h; μ: NR. Fault 4 s; detection/switch 4.1 s.	Peak/RMS: wheel-angle error 0.0112/0.0031 rad; sideslip-angle error 0.0016/0.0007 rad; yaw-rate error 0.0329/0.0114 rad/s.	Vehicle lateral-response tracking is quantified; footprint clearance is not reported.
Lu and Tian [22] Simulation	Drive/steering failures; remaining wheel actuators reallocated	Double lane change; initial target 80 km/h; μ = 1. Faults present from the start; 255 combinations.	Selected case: peak tracking error 1.368 m without speed adaptation; adaptive case averages about 65 km/h. Thirty combinations fail the maneuver.	Shows speed-demand adaptation. Unexpected-fault diagnosis and a contained stop were not tested.
Han et al. [37] Simulation	Steering failure; differential wheel drive and torque allocation	Single lane change; 100 km/h; μ = 0.8. Failure injected at 3 s; diagnostic delay not evaluated.	Maximum lateral deviation 0.0917 m; maximum yaw-rate deviation 0.227°/s.	Vehicle tracking quantified for the modeled maneuver.
Wang et al. [80] Steering rig/HIL	Relay-induced winding open circuit; healthy winding supplies torque	Double lane change; simulated speed 80 km/h; μ: NR. Winding fault around 3 s.	Steering reversal and current disturbance precede restored balance on the healthy winding.	Physical steering and drive circuits; vehicle plant simulated. Numerical vehicle-path and yaw/sideslip errors: NR.
Li et al. [81] Controller HIL	Effectiveness and bias faults; healthy independent steering channels	Step input (3 s) and sine input; speed: NR; μ: NR. Known-fault step case; observer-estimated sine case.	Yaw/sideslip responses track the reference more closely than baselines. Reported PID displacement errors at 3 s: 0.8/0.7 m.	Baseline displacement is not residual FTC error. Vehicle-motion comparisons are plotted; a numerical FTC residual or clearance is NR.

Table 6. *Cont.*

Study/Evidence	Fault and Surviving Actuation	Maneuver, Speed, Friction; Fault Information	Reported Outcome	Vehicle-Level Interpretation
Wang et al. [60] Controller HIL	Time-varying additive steering fault; steering and wheel-torque compensation	Double lane change: 50 km/h, μ = 0.8. S-turn: 80 km/h, μ = 0.5. Integrated fault observer; CarSim plant.	Lane-change peak lateral error 0.1035 → 0.0295 m (separate → integrated FTC); fault estimation about 0.5 → 0.3 s.	S-turn peak lateral error 7.68 → 2.56 m. Both results are vehicle-model outcomes with a physical controller. Speed, maneuver, and friction all differ from the lane-change case.
Zhang et al. [82] Component HIL	Single-motor effectiveness reduction; healthy dual-motor steering capacity	Steering step/sine inputs; HIL speed and μ: NR. Companion simulations: 70 km/h, μ = 0.8. Fault after 5 s; coupled estimation.	Source-reported angle-tracking efficiency: AFTC 96.6–94.0%; conventional MPC 74.1–41.7% as severity increases.	Controller and steering assembly physical; PXI vehicle model. Numerical vehicle-level motion/clearance outcomes: NR.
Seiffer et al. [48] Scaled vehicle	Steering-actuator failure; wheel-selective drives provide differential steering	Modified double lane change; 5.5 m/s; 1:1.5 vehicle; μ: NR. Actuator state supplied to allocation.	Faulted lateral peak/RMS 0.0612/0.0295 m; healthy 0.0597/0.0283 m. Minimum boundary distance 0.0330 m.	Physical maneuver continuation under the stated speed, scale, and supplied fault state.
Ha et al. [12] Full-size vehicle	Fixed front angle or torque loss; rear steering and drive/brake torque vectoring	Step and one-period sine input; 30 km/h; about 0.1 g; μ: NR. Separate fault-detection input.	Rear steering compensates tested fixed-angle cases; torque-loss response deteriorates, with partial recovery under combined control.	Vehicle trajectory/yaw responses reported; numerical residual summary: NR. Sideslip and corridor clearance not measured.

6.2. Speed Reduction and the Changing Recovery Envelope

For moderate sideslip and transients, the lateral acceleration required by a path is approximately $v^2\kappa$, where κ is curvature. Lu and Tian [22] test speed adaptation in CarSim–Simulink with drive and steering faults present from the start. In their selected combined-fault case, fixed-speed fault-tolerant control leaves a peak tracking error of 1.368 m at an initial target of 80 km/h. Adaptive velocity planning lowers the average speed to about 65 km/h and improves tracking. Across their 255 simulated fault combinations, 30 still fail to complete the double lane change. The study demonstrates a benefit of reducing demand, but does not test the transition from an unexpected fault to a controlled stop.

Braking and lateral recovery compete for tire capacity during the transient. Deceleration also transfers vertical load toward the front axle, changing both lateral-force capacity and the effectiveness of front and rear actuation. A heavy brake request can initially consume force needed for steering before the lower speed improves the situation. The trade-off depends on available distance, friction, axle loading, and brake distribution. Integrated steering and braking predictive-control studies clarify these couplings under nominal and uncertain high-speed conditions [87,100]. Their models provide useful foundations for fault recovery when the failed steering channel and the remaining authority are represented explicitly.

Roll motion adds another coupling because braking and cornering redistribute normal load. The publisher abstract of Qi et al. [59] reports adaptive predictive control combining differential steering, path tracking, and rollover prevention with simulation and HIL evaluation. Partitioned-cost control provides a related way to assign competing motion objectives [101].

As the vehicle approaches standstill, steering friction, brake release, and motor torque ripple become more prominent, while conventional slip-angle models become less suitable. A stopping maneuver therefore includes the final low-speed transition and wheel orientation. These conditions affect the stopping path, holding on a slope, and any subsequent restart.

6.3. Driver Interaction and Control Authority

Driver input remains relevant when an automated or assisted vehicle experiences a steering fault. A driver may respond to path departure by adding the handwheel angle while the recovery controller generates a yaw moment through wheel torque. Those actions can cooperate or oppose each other, depending on the failed channel and on the driver's interpretation of handwheel feedback. Driver-aware fault-tolerant control has addressed individual steering characteristics and auxiliary steering assistance [102,103]. Recovery assessment can represent driver input with a defined authority and response delay.

Game-based methods express driver–automation interaction through coupled objectives. Cooperative formulations account for actuator faults and uncertain driver behavior [104,105]. Koopman models and neural network Nash-game formulations extend this approach to steer-by-wire assistance [106,107]. The available steering action constrains both participants' decisions. A fault-dependent action set can therefore connect driver-intent estimation and shared control to the physical authority retained by the vehicle.

Handwheel feedback communicates the active recovery mode to the driver. Steer-by-wire separates this feedback from road-wheel actuation [1,4]. When braking supplies much of the yaw correction, feedback and control authority need to reflect the associated steering response and deceleration. The design also specifies whether the driver can modify the recovery path, request braking, or interrupt an automated maneuver.

Driver recognition and response add to the time before corrective input. Tests can separate the initial automatic response from later driver participation, with stated authority and response delay. This links assistance-control methods to the mechanical recovery conditions without treating driver recognition as instantaneous.

7. Evidence from Simulation and Experiments

7.1. Simulation, Hardware in the Loop, and Vehicle Tests

Table 6 compares 11 studies across software simulation, controller HIL, physical steering rigs with a simulated vehicle, and vehicle tests. Every row identifies the maneuver or input, speed, friction information, fault-information assumption, and available vehicle-level outcome. Component-only results are labeled explicitly. Supplementary Table S2 provides the associated fault, surviving-actuator, model, and validation extraction, together with three foundational studies. These cases cover different recovery mechanisms and operating conditions; their unequal metrics do not support a pooled ranking.

Fault-information assumptions separate three kinds of evaluation. Lu and Tian [22] impose faults from the start and assess the degraded controller. Ha et al. [12] use a separate fault-detection input, and Seiffer et al. [48] require actuator-state information for allocation. These studies test control after fault information is supplied. Kim and Kim [23], Wang et al. [60], and Zhang et al. [82] include fault estimation in the feedback loop. Huang et al. [18] also simulate detection and motor switching. An injected failure time is therefore not itself evidence of a tested diagnostic chain.

The HIL platforms in Figure 10 exercise different physical interfaces. Li et al. [81] use an embedded vehicle controller, CAN interfaces, and a real-time CarSim/VeriStand plant. Their step and sine-input cases compare known fault parameters with observer-estimated faults. Wang et al. [60] run the controller on dSPACE hardware and the CarSim vehicle model on an NI host, linked through CAN/PCAN. This setup tests estimator–controller

execution against a simulated vehicle. In both cases, reported vehicle motion depends on the plant model; these tests are not road-vehicle experiments.

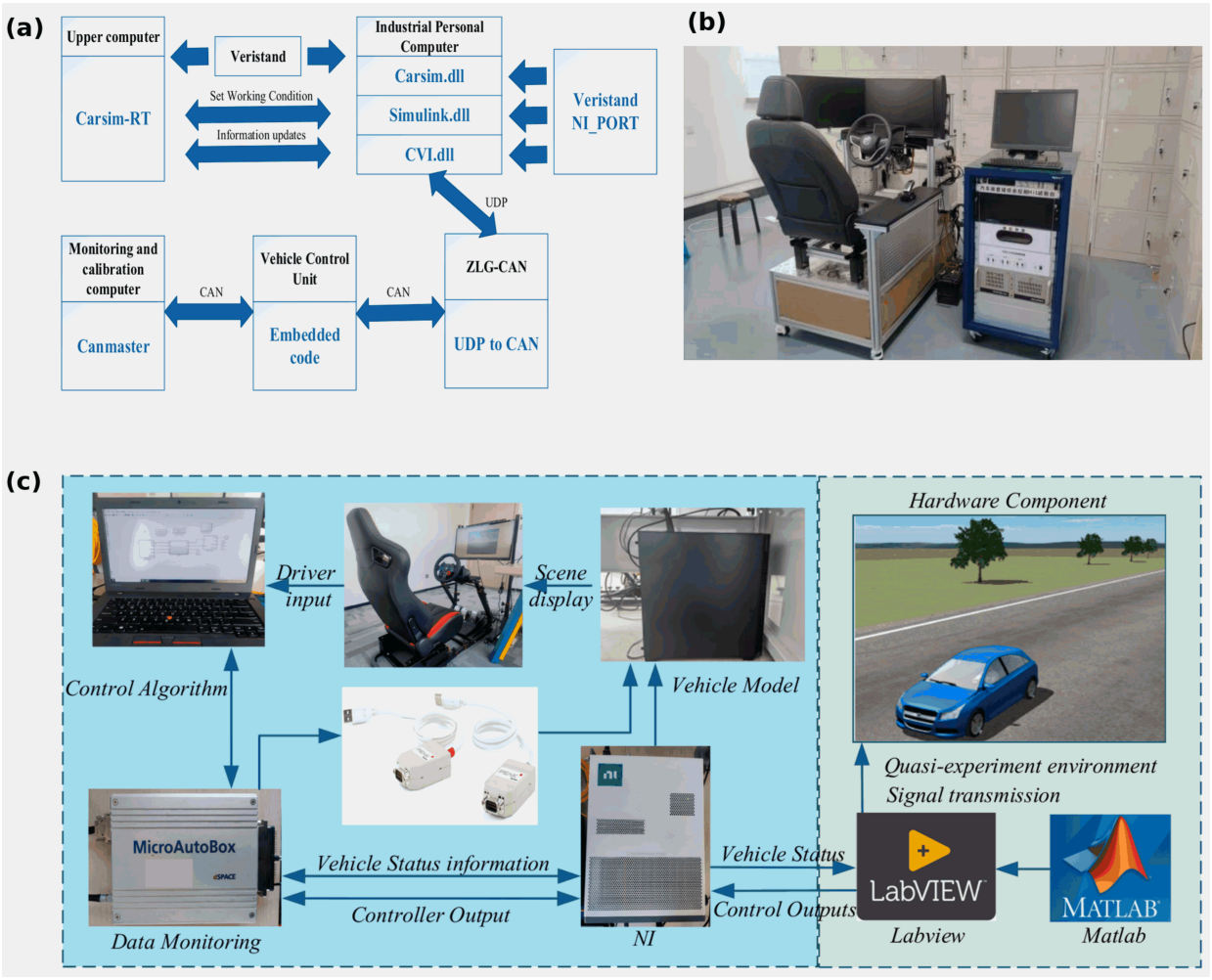


Figure 10. HIL platforms for steering-fault control. (**a**) Controller–plant architecture and (**b**) test rig (Reproduced from Figure 3a,b of Li et al. [81]). (**c**) Integrated fault-estimation and control platform (Reproduced from Figure 4 of Wang et al. [60]). Reproduced under CC BY 4.0.

Component HIL includes physical steering hardware. Zhang et al. [82] connect a dual-motor controller and steering actuator assembly to a PXI vehicle model. The tests exercise fault estimation and angle tracking under injected motor-effectiveness reductions. Wang et al. [80] use a steering rig and relay-induced winding open circuits; the surviving winding restores steering after a reversal transient. Neither setup physically reproduces the complete tire–road interaction. Liu et al. [36] evaluate dual-motor synchronization using simulated motor responses. Xu et al. [71] report simulation and HIL in the abstract, without sufficient accessible setup detail for inclusion in the hardware comparison.

Ha et al. [12] test a Hyundai sedan with rear steering, wheel brakes, and drive actuation. Physical tests use step and one-period sine inputs at 30 km/h and approximately 0.1 g nominal lateral acceleration. Under fixed-angle failure, rear-steering-based compensation is effective in those maneuvers. Under loss of torque, unintended front-wheel motion weakens rear steering alone, and combined rear steering and torque vectoring provides partial compensation. The higher-speed and broader cornering comparisons are simulation results. The vehicle tests do not measure sideslip or establish a road-corridor recovery boundary.

Seiffer et al. [48] test a 1:1.5 demonstrator at 5.5 m/s in a modified double lane change. After steering-actuator failure, peak and RMS crosstrack errors are 0.0612 and 0.0295 m,

compared with 0.0597 and 0.0283 m without failure. The reported minimum lane-boundary distance is 0.0330 m. This is direct vehicle evidence of maneuver continuation in the tested configuration. Steering-angle error is larger than in simulation, with friction and breakaway torque affecting reversals. Fault-state information is supplied to the allocator; diagnostic latency is not established by this test.

Ha et al. [13] report vehicle measurements used to validate the differential-braking model for negative kingpin offset. Their wider offset range and closed-loop controller comparisons are evaluated in the vehicle model and CarMaker. This distinction between vehicle-based model validation and simulated controller evaluation is stated in the publisher abstract.

7.2. Quantitative Results and Operating Conditions

Meléndez-Useros et al. [21] simulate a double lane change at 25 m/s. The healthy reference already has a lateral RMS error of 0.2497 m and a peak error of 0.7800 m. At steering effectiveness 0.1, compensation reduces RMS error from 0.8071 to 0.3983 m, while the compensated peak remains 1.2064 m. With 3° steering saturation, RMS decreases from 0.6643 to 0.3519 m, and the compensated peak remains 1.0751 m. At effectiveness 0.3, RMS decreases from 0.4113 to 0.3030 m, but peak error increases from 0.8960 to 0.9321 m. These results show both the benefit of compensation and the remaining excursion relative to an imperfect healthy baseline. Road containment additionally requires the vehicle footprint and available clearance.

Kim and Kim [23] evaluated steering biases during a simulated double lane change at 100 km/h. Constant-bias detection times were 606.3 ms at 1° and 76.6 ms at 5°. Intermittent-bias detection times were 166.8 and 46.6 ms at the same amplitudes. Drifting-bias detection times were 11,616.0 and 8177.1 ms, respectively. The amplitude dependence links diagnosis speed to residual separation: a small persistent bias can remain close to model error while its effect on the path accumulates. In the 1° intermittent-bias case, the reported lateral RMS improvement was −6.941%, indicating a slight increase in tracking error after compensation. This small-fault result is distinct from the separate friction-and-mass robustness comparison.

Huang et al. [18] simulate a variable-speed single lane change from 80 to 100 km/h, a motor-2 short circuit at 4 s, and switching at 4.1 s. Their robust LQR controller produces peak/RMS front-wheel angle errors of 0.0112/0.0031 rad. The corresponding vehicle-level sideslip-angle errors are 0.0016/0.0007 rad, and yaw-rate errors are 0.0329/0.0114 rad/s. These are simulated tracking errors relative to the desired responses. The source does not report a footprint-clearance metric or a tire–road friction coefficient for this case.

7.3. Scenarios for Evaluating Recovery Boundaries

Table 7 sets out our proposed comparison scenarios. Steering reversals target the breakaway and rate effects observed on the demonstrator [48]. Combined faults and braking maneuvers target the loss of force reserve seen in the speed-adaptation study [22]. The common boundary and timing measurements proposed below would allow these mechanisms to be compared on the same recovery task.

Fault onset should be varied before a turn, near peak lateral demand, and during steering reversal. These phases have different force and rate reserves. Reporting the onset state, diagnostic delay, and peak footprint excursion would show which part of the transition sets the recovery limit.

Split-friction transitions test whether left–right force asymmetry is represented during recovery [54]. Tests should distinguish a controller supplied with the actual friction change from one that estimates it online. This separates allocation capability from the effect of a delayed model update.

Table 7. Proposed scenarios for assessing recovery boundaries.

Scenario	Fault Variation	Dominant Mechanism	Measurements
Straight-road lane holding	Small bias; drifting bias	Accumulated departure and delayed detection	Residuals, heading, footprint clearance
Constant-radius corner	Nonzero locked angle	Persistent imbalance and directional capability	Wheel angles, lateral forces, yaw reserve
Double lane change	Fault before peak demand or reversal	Rate limits and transient saturation	Onset state, peak departure, achieved torque
Braking in a turn	Steering loss with commanded deceleration	Combined tire demand and load transfer	Wheel slip, normal load, path and speed
Split-friction transition	Fault before or during surface change	Asymmetric force availability	Estimated friction, wheel force, yaw response
Reduced-speed controlled stop	Lock or freely moving rack	Low-speed steering and brake transition	Stopping path, final heading, wheel orientation
Repeated steering input	Partial steering or drive degradation	Sustained reserve and heating	Current, temperature, rate-limit activity

Payload and tire variation change the axle reserves and yaw response. Robust and active fault-tolerant tracking methods address these uncertainties through model bounds or adaptation [108,109]. Common mass, load-distribution, and tire conditions are needed to compare their effects on recovery.

7.4. Metrics over the Complete Transition

For a common recovery comparison, we propose recording fault onset, recognition, command transfer, and the terminal state on one time base. Figure 11 organizes the proposed measurements by hardware level. The record extends through settling to distinguish a short corrective pulse from sustained steering capability.

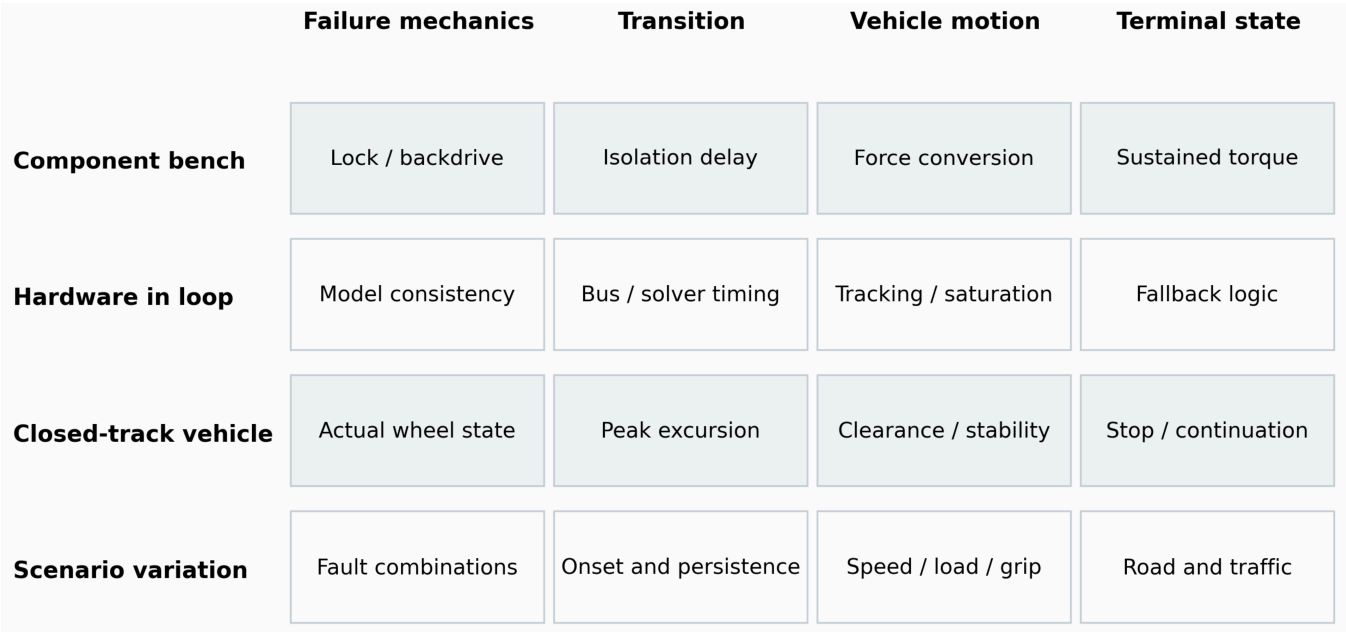


Figure 11. Proposed validation measurements across hardware levels and recovery phases.

We propose minimum signed footprint clearance as the road-containment measure: the minimum distance between the complete vehicle footprint and the road boundary over the transition, positive inside the permitted corridor and negative after a boundary

crossing. The footprint includes overhangs and changes with heading. This extends the lane-boundary-distance reporting in the demonstrator study [48] into a common comparison protocol. Peak and RMS tracking errors describe reference following; yaw rate and sideslip describe lateral response. The protocol records these quantities with speed, wheel angles, and achieved wheel torques. Replanned tracking uses the new reference, while clearance remains referenced to the road.

The timing record should also identify the safe-state or emergency-operation endpoint defined in Section 4.3 and report the remaining FTTI margin [72]. Clearance, yaw response, and achieved wheel torques should be evaluated over that complete interval. For a stopping maneuver, the terminal-state record should extend to standstill [75].

8. Research Priorities

8.1. Connecting Electrical Diagnosis to Mechanical Capability

The comparisons expose a gap between estimating a mathematical fault and identifying the mechanical state needed for recovery. Bias observers evaluate amplitude and detection delay [23]; complete-failure vehicle tests show that fixed angle and torque loss produce different responses [12]. Wheel-corner diagnosis and adaptive coordination provide related methods [110,111]. The next comparison should test whether the same sensing arrangement can distinguish lock, free motion, and reduced torque, then quantify how that decision changes the selected recovery action.

The relevant outputs are the measured wheel-angle evolution, the time at which the mechanical state is identified, and the resulting minimum road clearance. Motor-only sensing and independent road-wheel sensing can be compared on the same failed mechanism. This would connect diagnostic improvement to a vehicle outcome rather than to classification accuracy alone.

8.2. Sharing Capability Between Allocation and Planning

Known actuator-state information supports the transition demonstrated by Seiffer et al. [48], while Lu and Tian [22] assess adaptation with faults already present. Neither study isolates the effect of an uncertain detection-to-actuation delay on the planning boundary. A common comparison should vary that delay while keeping the allocator and fault fixed, and compare static force bounds with state- and rate-dependent reachable bounds. The measured outputs would be infeasible requests, the actual fallback command, and minimum clearance.

The reported winding-failure tests show torque transfer and a short reversal transient [80]. They do not establish how long substitute actuation can be sustained under repeated correction. Continued travel therefore needs measurements of temperature, current limits, tire demand, and any thermal derating over a stated duration. A controlled-stop comparison should additionally include the low-speed steering and brake transition.

Table 8 links our proposed comparisons to published findings.

Table 8. Evidence gaps and proposed comparisons.

Published Finding	Unresolved Comparison	Proposed Test and Output
Rear-steering performance changes between fixed angle and torque loss in low-speed sedan tests [12]	Recovery boundary across the two mechanical states	Same vehicle, lock angle, speed, and friction sweep; record wheel angles and footprint clearance
Demonstrator transition uses supplied actuator-state information [48]; bias detection depends on amplitude [23]	Effect of uncertain diagnosis and transfer delay	Measured/injected delay with the same allocator; log selected mode, applied command, and peak departure

Table 8. *Cont.*

Published Finding	Unresolved Comparison	Proposed Test and Output
Reduced RMS can coexist with large peaks [21]; a larger HIL residual occurs under combined high-speed, low-friction S-turn conditions [60]	Tracking improvement versus road containment	Report RMS, peak error, yaw/sideslip, and minimum footprint clearance under common road boundaries
Speed adaptation improves tracking but 30 simulated combinations remain incomplete [22]	Feasible continuation versus a contained stop	Compare reduced-speed continuation and stopping from the same post-fault state; measure terminal position, speed, and heading
Winding transfer restores steering after a reversal transient on the rig [80]	Duration of usable substitute actuation	Repeated correction with current, temperature, derating, and low-speed steering measurements
Physical component HIL verifies angle tracking [82]; scaled vehicle tests expose breakaway effects [48]	Transfer of the same fault model between platforms	Use matching fault injection across component HIL and vehicle tests; compare actual angle, torque, and transient error

8.3. Reproducible Comparisons Across Recovery Mechanisms

A common benchmark should preserve the physical fault across simulation, component HIL, and vehicle testing. It should specify whether steering is locked or unpowered, the surviving actuator bounds and rates, and the fault signals supplied to each controller. The scaled demonstrator [48] and low-speed sedan tests [12] provide distinct experimental anchors; neither defines a universal recovery envelope.

A fixed degraded controller, reconfigured allocation, and speed-adaptive planning provide useful baselines under the same fault. Trials should include marginal and unsuccessful maneuvers. The 30 incomplete simulated cases reported by Lu and Tian [22] show why successful tracking examples alone cannot define continued-travel capability.

For continuation, tests need a stated speed range, route demand, and operating duration. For stopping, they need a feasible deceleration trajectory and a terminal footprint inside the road corridor. Publishing synchronized fault signals, actual wheel angles, achieved torques, and clearance would allow the mechanism of a failed trial to be assessed. Experimental sensor-fault validation offers a related measurement-based approach [70].

9. Conclusions

Steering-failure recovery depends on the mechanical state left by the fault. A lock preserves the wheel orientation and creates a persistent force constraint. Torque loss allows the wheel angle to evolve under road forces; rear-steering compensation that works for a fixed angle can then be much less effective. Reduced effectiveness retains a compensable channel only within its remaining torque, current, and rate limits.

Vehicle evidence supports selected forms of continuation. Low-speed sedan tests show the different responses of fixed-angle and torque-loss failures under rear steering and combined torque vectoring [12]. A 1:1.5 demonstrator maintains a modified double lane change after steering-actuator failure with externally supplied actuator-state information [48]. HIL studies test controller execution or physical steering components against a simulated vehicle. These results establish different parts of recovery and should retain their platform and operating conditions.

Simulation extends the comparison to severe gain loss, saturation, and multiple faults. It shows that lower RMS error can coexist with substantial peak departure, and that speed adaptation improves some maneuvers while leaving other fault combinations infeasible. Static force availability therefore needs to be combined with the response time, steering

dynamics, and a feasible motion reference. Tracking accuracy, lateral stability, and road containment remain separate outcomes. The available comparisons support short maneuvers under stated faults; continued travel and controlled stopping still require vehicle tests spanning diagnosis, transfer, sustained loading, and the final low-speed phase.

Supplementary Materials: The following supporting information can be downloaded at https://www.mdpi.com/article/10.3390/wevj17120632/s1.

Author Contributions: Writing—original draft preparation, L.Z.; writing—review and editing, L.C., R.R.; supervision, R.R. Conceptualization, L.Z. and R.R.; investigation, L.C.; resources, R.R.; data curation, L.Z.; writing—original draft preparation, L.Z.; writing—review and editing, R.R. and L.C.; supervision, L.C.; funding acquisition, L.C. All authors have read and agreed to the published version of the manuscript.

Funding: This research was funded by Shandong Province Higher Education Institutions Marine Vessel Special Motor Key Technology Development and Component Manufacturing University-Enterprise Collaborative Innovation Center grant number [PT2025KJS005].

Data Availability Statement: No new data were created or analyzed in this study. Data sharing is not applicable to this article.

Acknowledgments: During the preparation of this manuscript, the authors used ChatGPT version 6.0 for for English language and grammatical corrections. The authors have reviewed and edited the output and take full responsibility for the content of this publication.

Conflicts of Interest: The authors declare no conflict of interest.

References

1. Huang, C.; Naghdy, F.; Du, H.; Huang, H. Fault tolerant steer-by-wire systems: An overview. *Annu. Rev. Control* **2019**, *47*, 98–111. [CrossRef]
2. Mortazavizadeh, S.A.; Ghaderi, A.; Ebrahimi, M.; Hajian, M.; Ebrahimi, M. Recent developments in the vehicle steer-by-wire system. *IEEE Trans. Transp. Electrif.* **2020**, *6*, 1226–1235. [CrossRef]
3. Hang, P.; Chen, X. Towards autonomous driving: Review and perspectives on configuration and control of four-wheel independent drive/steering electric vehicles. *Actuators* **2021**, *10*, 184. [CrossRef]
4. Lu, Y.; Zhong, J.; Khoshnevisan, L.; Sun, C.; Khajepour, A. A review on vehicle steer-by-wire control systems. *Veh. Syst. Dyn.* **2025**, *ahead of print*. [CrossRef]
5. Perdana, M.A.P.; Budiman, A.C.; Ristiana, R.; Muharam, A.; Ismail, K.; Kurnia, M.R.; Amin; Huda, N.; Kaleg, S.; Hapid, A. Control strategies for steer-by-wire systems: An overview. *Technologies* **2025**, *13*, 6. [CrossRef]
6. Fekih, A.; Devariste, D. A fault-tolerant steering control design for automatic path tracking in autonomous vehicles. In Proceedings of the 2013 American Control Conference (ACC), Washington, DC, USA, 17–19 June 2013; pp. 5146–5151. [CrossRef]
7. Wada, N.; Fujii, K.; Saeki, M. Reconfigurable fault-tolerant controller synthesis for a steer-by-wire vehicle using independently driven wheels. *Veh. Syst. Dyn.* **2013**, *51*, 1438–1465. [CrossRef]
8. Yim, S. Fault-tolerant yaw moment control with steer—And brake-by-wire devices. *Int. J. Automot. Technol.* **2014**, *15*, 463–468. [CrossRef]
9. Dominguez-Garcia, A.D.; Kassakian, J.G.; Schindall, J.E. A backup system for automotive steer-by-wire, actuated by selective braking. In Proceedings of the IEEE 35th Annual Power Electronics Specialists Conference, Aachen, Germany, 20–25 June 2004; Volume 1, pp. 383–388. [CrossRef]
10. Mihály, A.; Gáspár, P. Reconfigurable fault-tolerant control of in-wheel electric vehicles with steering system failure. *IFAC-PapersOnLine* **2015**, *48*, 49–54. [CrossRef]
11. Zhang, L.; Wang, Z.H.; Sun, F.C.; Wang, Z.P. Fault-tolerant control for intelligent four-wheel-independently-actuated electric vehicles under complete steer-by-wire system failure. *J. Mech. Eng.* **2021**, *57*, 141–152. [CrossRef]
12. Ha, Y.; Jeon, S.; Sorniotti, A.; Woo, S. Comparative study of fault-tolerant control strategies for complete steer-by-wire failures. *Control Eng. Pract.* **2026**, *170*, 106812. [CrossRef]
13. Ha, Y.; Jeon, S.; Park, H.; Sorniotti, A.; Woo, S. Capability analysis of fault-tolerant control with differential braking for steer-by-wire failure. *IEEE Access* **2025**, *13*, 122354–122375. [CrossRef]
14. Xia, G.; Zhang, B.; Zhang, Y.; Wei, H.; Khajepour, A. Fault-tolerant control of off-road vehicle steering based on motor torque compensation and differential steering. *Proc. Inst. Mech. Eng. D J. Automob. Eng.* **2026**, *ahead of print*. [CrossRef]

15. Huang, B.; Zhao, S.; Wei, J.; Zhang, G.; Wei, X. A review of coordinated torque allocation for energy efficiency and stability in distributed-drive electric vehicles. *World Electr. Veh. J.* **2026**, *17*, 431. [CrossRef]
16. Stolte, T. Actuator fault-tolerant vehicle motion control: A survey. *arXiv* **2021**, arXiv:2103.13671. [CrossRef]
17. Huang, C.; Huang, H.; Naghdy, F.; Du, H.; Ma, D. Actuator fault tolerant control for steer-by-wire systems. *Int. J. Control* **2021**, *94*, 3123–3134. [CrossRef]
18. Huang, J.; Mao, J.; Yang, R.; Qin, P.; Ye, L.; Huang, W. Fault-tolerant control and switching mechanism of dual-motor steer-by-wire systems under coupled communication delays and faults. *World Electr. Veh. J.* **2026**, *17*, 228. [CrossRef]
19. Hu, H.; Tang, M.; Chen, G.; Gao, Z.; Wang, X.; Gao, F. Design of a fault-tolerant control algorithm for four-wheel steering vehicle steering locking based on dynamic model reconstruction. *SAE Int. J. Veh. Dyn. Stab. NVH* **2025**, *9*, 10-09-04-0036. [CrossRef]
20. Sung, J.; Choi, S.; Huh, K. A differential brake-actuated steering system for redundancy of steer-by-wire. *IEEE Trans. Intell. Veh.* **2024**, *9*, 993–1004. [CrossRef]
21. Meléndez-Useros, M.; Viadero-Monasterio, F.; Jiménez-Salas, M.; López-Boada, M.J. Static output-feedback path-tracking controller tolerant to steering actuator faults for distributed driven electric vehicles. *World Electr. Veh. J.* **2025**, *16*, 40. [CrossRef]
22. Lu, A.; Tian, G. Unified fault-tolerant control and adaptive velocity planning for 4WID-4WIS vehicles under multi-fault scenarios. *Actuators* **2024**, *13*, 407. [CrossRef]
23. Kim, H.; Kim, W. Active fault-tolerant control for steering actuator bias in autonomous vehicles using adaptive sliding mode observer. *Sensors* **2026**, *26*, 1680. [CrossRef] [PubMed]
24. Zou, S.; Zhao, W.; Liang, W.; Wang, C.; Chen, F. Fault diagnosis and fault-tolerant compensation strategy for wheel angle sensor of steer-by-wire vehicle via extended Kalman filter. *IEEE Sens. J.* **2022**, *22*, 1756–1766. [CrossRef]
25. Yang, C.; Wang, Q.; Wang, W.; Gao, Y.; Zhang, Y.; Zhang, R. A fault estimation and fault-tolerant operation scheme design under simultaneous actuator and sensor faults for steer-by-wire system. *Veh. Syst. Dyn.* **2026**, *64*, 975–1002. [CrossRef]
26. Wang, Q.; Yang, C.; Zhang, Y.; Gao, Y.; Fang, J.; Wang, W. Integrated fault-tolerant control scheme for steer-by-wire systems based on steering motor and steering angle sensor fault estimation. *IEEE Trans. Ind. Electron.* **2026**, *ahead of print*. [CrossRef]
27. Huang, C.; Naghdy, F.; Du, H. Fault tolerant sliding mode predictive control for uncertain steer-by-wire system. *IEEE Trans. Cybern.* **2019**, *49*, 261–272. [CrossRef] [PubMed]
28. Zhao, L.; Zhao, X.; Li, H. Rack force fault tolerance estimation of steer-by-wire system under different resolver faults based on sensor flows. *Control Eng. Pract.* **2024**, *147*, 105941. [CrossRef]
29. Mi, J.; Wang, T.; Lian, X. A system-level dual-redundancy steer-by-wire system. *Proc. Inst. Mech. Eng. D J. Automob. Eng.* **2021**, *235*, 3002–3025. [CrossRef]
30. Huang, C.; Li, L. Architectural design and analysis of a steer-by-wire system in view of functional safety concept. *Reliab. Eng. Syst. Saf.* **2020**, *198*, 106822. [CrossRef]
31. Shi, G.; Qiao, P.; Sang, D.; Wang, S.; Song, M. Synchronous and fault-tolerance control for dual-motor steer-by-wire system of commercial vehicle. *Proc. Inst. Mech. Eng. D J. Automob. Eng.* **2024**, *238*, 1964–1980. [CrossRef]
32. Xu, K.; Liang, W.; Zhao, W.; Wang, C.; Zou, S.; Zhou, X. Vehicle stability and synchronization control of dual-motor steer-by-wire system considering multiple uncertainties. *IEEE Trans. Transp. Electrif.* **2024**, *10*, 3092–3104. [CrossRef]
33. Zou, S.; Zhao, W.; Wang, C.; Liang, W.; Chen, F. Tracking and synchronization control strategy of vehicle dual-motor steer-by-wire system via active disturbance rejection control. *IEEE/ASME Trans. Mechatron.* **2023**, *28*, 92–103. [CrossRef]
34. Shi, G.-B.; Guo, C.; Wang, S.; Liu, T.-Y. Angle tracking and fault-tolerant control of steer-by-wire system with dual three-phase motor for autonomous vehicle. *IEEE Trans. Intell. Transp. Syst.* **2024**, *25*, 5842–5853. [CrossRef]
35. Wang, X.; Pan, L.; Tian, Y.; Liu, Y.; Li, L. Adaptive fault-tolerant fixed-time sliding mode tracking control for steer-by-wire system with dual-three-phase PMSM. *IEEE Trans. Veh. Technol.* **2025**, *74*, 7554–7564. [CrossRef]
36. Liu, J.; Yang, Z.; Xu, X.; Zhou, T.; Zhou, Y. Research on fault-tolerant synchronous control of dual motors for wire-controlled steering based on average deviation coupled fuzzy PID. *Machines* **2026**, *14*, 495. [CrossRef]
37. Han, Q.; Liu, C.; Zhao, J.; Liu, H. The fault-tolerant control strategy for the steering system failure of four-wheel independent by-wire steering electric vehicles. *World Electr. Veh. J.* **2025**, *16*, 183. [CrossRef]
38. Kirli, A.; Chen, Y.; Okwudire, C.E.; Ulsoy, A.G. Torque-vectoring-based backup steering strategy for steer-by-wire autonomous vehicles with vehicle stability control. *IEEE Trans. Veh. Technol.* **2019**, *68*, 7319–7328. [CrossRef]
39. Hu, C.; Wang, R.; Yan, F.; Karimi, H.R. Robust composite nonlinear feedback path-following control for independently actuated autonomous vehicles with differential steering. *IEEE Trans. Transp. Electrif.* **2016**, *2*, 312–321. [CrossRef]
40. Hu, C.; Qin, Y.; Cao, H.; Song, X.; Jiang, K.; Rath, J.J.; Wei, C. Lane keeping of autonomous vehicles based on differential steering with adaptive multivariable super-twisting control. *Mech. Syst. Signal Process.* **2019**, *125*, 330–346. [CrossRef]
41. Tian, J.; Yang, M. Hierarchical control of differential steering for four-in-wheel-motor electric vehicle. *PLoS ONE* **2023**, *18*, e0285485. [CrossRef] [PubMed]
42. Römer, J.; Kautzmann, P.; Frey, M.; Gauterin, F. Reducing energy demand using wheel-individual electric drives to substitute EPS-systems. *Energies* **2018**, *11*, 247. [CrossRef]

43. Kwon, B.-S. Fault-tolerant control strategy for steer-by-wire vehicles using rear-wheel steering. *J. Inst. Control Robot. Syst.* **2023**, *29*, 289–293. [CrossRef]
44. Yu, C.; Zheng, Y.; Shyrokau, B.; Ivanov, V. MPC-based path following design for automated vehicles with rear wheel steering. In Proceedings of the 2021 IEEE International Conference on Mechatronics (ICM), Kashiwa, Japan, 7–9 March 2021; pp. 1–6. [CrossRef]
45. Feng, H.; Tao, Y.; Feng, J.; Zhang, Y.; Xue, H.; Wang, T.; Xu, X.; Chen, P. Fault-tolerant collaborative control of four-wheel-drive electric vehicle for one or more in-wheel motors' faults. *Sensors* **2025**, *25*, 1540. [CrossRef] [PubMed]
46. Tang, H.; Chen, Y.; Zhou, A. Actuator fault-tolerant control for four-wheel-drive-by-wire electric vehicle. *IEEE Trans. Transp. Electrif.* **2022**, *8*, 2361–2373. [CrossRef]
47. Lu, A.; Li, R.; Yu, Y.; Ji, W.; Hou, Y.; Tian, G. *Impacts of Dynamic Toe Angle Variations on Four-Wheel Independent Steering Control and Their Optimization Strategies*; SAE Technical Paper 2024-01-2321; SAE International: Warrendale, PA, USA, 2024. [CrossRef]
48. Seiffer, A.; Frey, M.; Gauterin, F. Control allocation approach using differential steering to compensate for steering actuator failure. *IEEE Open J. Intell. Transp. Syst.* **2024**, *5*, 756–773. [CrossRef]
49. Lu, A.; Yu, Y.; Li, R.; Tian, G. Advanced fault-tolerant strategies and quantification for 4WID-4WIS vehicles with actuator faults. *Proc. Inst. Mech. Eng. D J. Automob. Eng.* **2026**, *240*, 3712–3725. [CrossRef]
50. Wang, W.; Sun, R.; Yang, C.; Zhang, Y.; Li, H.; Liu, H.; Yao, S. Capability-based hierarchical fault-tolerant control scheme for four-wheel-independent-drive electric vehicles under actuator faults. *IEEE Trans. Veh. Technol.* **2025**, *74*, 11906–11917. [CrossRef]
51. Hu, J.; Jia, M.; Xiao, F.; Fu, C.; Zheng, L. Motor vector control based on speed-torque-current map. *Appl. Sci.* **2020**, *10*, 78. [CrossRef]
52. Wassiliadis, N.; Steinsträter, M.; Schreiber, M.; Rosner, P.; Nicoletti, L.; Schmid, F.; Ank, M.; Teichert, O.; Wildfeuer, L.; Schneider, J.; et al. Quantifying the state of the art of electric powertrains in battery electric vehicles: Range, efficiency, and lifetime from component to system level of the Volkswagen ID.3. *eTransportation* **2022**, *12*, 100167. [CrossRef]
53. Heydrich, M.; Ricciardi, V.; Ivanov, V.; Mazzoni, M.; Rossi, A.; Buh, J.; Augsburg, K. Integrated braking control for electric vehicles with in-wheel propulsion and fully decoupled brake-by-wire system. *Vehicles* **2021**, *3*, 145–161. [CrossRef]
54. Ji, Y.-H.; Liu, Y.-C. Force allocation control for distributed drive electric vehicles under split-friction regions and actuator faults. *ISA Trans.* **2022**, *129*, 398–412. [CrossRef] [PubMed]
55. Oh, S.C.; Song, T.J.; Kim, M.J.; Oh, K.S. Adaptive model predictive fault-tolerant control for four-wheel independent steering vehicles with sensitivity estimation. *Int. J. Automot. Technol.* **2023**, *24*, 829–850. [CrossRef]
56. Koysuren, K.; Cakmakci, M. A fault-tolerant model predictive controller with reconfiguration for optimal lateral stability in over-actuated electric vehicles. *IEEE Trans. Intell. Veh.* **2025**, *10*, 1353–1364. [CrossRef]
57. Shi, Y.; Yao, Q.; Zhu, Z. Trajectory tracking control for 4-WID vehicles under steering failure based on a fault-tolerant feasible region and reference trajectory reshaping. *Int. J. Automot. Technol.* **2026**, *ahead of print*. [CrossRef]
58. Stolte, T.; Loba, M.; Nee, M.; Wu, L.; Maurer, M. Toward fault-tolerant vehicle motion control for over-actuated automated vehicles: A non-linear model predictive approach. *IEEE Access* **2023**, *11*, 10499–10519. [CrossRef]
59. Qi, G.; Yue, M.; Liu, Y.; Xu, M.; Pang, L. Adaptive mpc-based path tracking integrated control for distributed drive electric vehicles with rollover prevention under steering failure. *Asian J. Control* **2026**, *28*, 1896–1910. [CrossRef]
60. Wang, F.; Chu, W.; Zhu, X. Integrated fault estimation and fault-tolerant control for drive-by-wire steering systems in four-wheel independent drive vehicles. *Sensors* **2026**, *26*, 4185. [CrossRef] [PubMed]
61. Sentouh, C.; Fouka, M.; Rath, J.J.; Popieul, J.-C. Adaptive observer-based output feedback FTC for nonlinear interconnected vehicle dynamics with unknown actuator faults. *IEEE Trans. Intell. Veh.* **2025**, *10*, 2806–2817. [CrossRef]
62. Yu, M.; Zeng, Q.; Wang, H.; Zhu, M.; Yan, X.; Jiang, W. Dual observer-based active fault-tolerant control for steer-by-wire system with additive actuator and sensor faults. *J. Braz. Soc. Mech. Sci. Eng.* **2026**, *48*, 607. [CrossRef]
63. Zhang, X.; Chen, J.; Su, L.; Gong, G.; Zhang, F. Active fault tolerance for sensor failures in steer-by-wire systems via multi-model adaptive Kalman filter. *IEEE Trans. Veh. Technol.* **2025**, *74*, 5442–5452. [CrossRef]
64. He, S.; Xu, X.; Xie, J.; Wang, F.; Liu, Z.; Zhao, F. Fault detection and fault-tolerant control of autonomous steering system for intelligent vehicles combining Bi-LSTM and SPRT. *Measurement* **2023**, *212*, 112708. [CrossRef]
65. Lan, D.; Yu, M.; Huang, Y.; Ping, Z.; Zhang, J. Fault diagnosis and prognosis of steer-by-wire system based on finite state machine and extreme learning machine. *Neural Comput. Appl.* **2022**, *34*, 5081–5095. [CrossRef]
66. Meléndez-Useros, M.; Viadero-Monasterio, F.; Jiménez-Salas, M.; López-Boada, M.J. Active steering fault diagnosis via integrated LSTM-based sensor detection and robust actuator fault estimation. *Reliab. Eng. Syst. Saf.* **2026**, *265*, 111573. [CrossRef]
67. Jiang, H.; Yang, N.; Liu, T.; Wang, J.; Mizuno, K.; Chen, M.; Zheng, J. Fault-tolerant control of steer-by-wire system based on Gaussian process regression. *Trans. Inst. Meas. Control* **2026**, *48*, 2115–2127. [CrossRef]
68. Tian, C.; Huang, C.; Huang, H.; Zhao, J. Fault-tolerant path tracking control for electric vehicles with steering actuator faults via learning-based fault detection. In Proceedings of the 2024 IEEE 22nd International Conference on Industrial Informatics (INDIN), Beijing, China, 18–20 August 2024; pp. 1–6. [CrossRef]

69. Lu, Y.; Li, G.; Yue, Y.; Wang, Z. Fault detection and data-driven optimal adaptive fault-tolerant control for autonomous driving using learning-based SMPC. *IEEE Trans. Intell. Veh.* **2024**, *ahead of print*. [CrossRef]
70. May, M.P.; Henning, K.-U.; Sawodny, O. Experimental validation of sensor fault estimation for vehicle dynamics with a nonlinear tire model. *Control Eng. Pract.* **2023**, *141*, 105725. [CrossRef]
71. Xu, X.; Wu, Z.; He, S.; Su, P.; Zhao, F. Fault detection and fault-tolerant control of dual-motor autonomous steering system. *Trans. Inst. Meas. Control* **2024**, *46*, 2984–2995. [CrossRef]
72. *ISO 26262-1:2018*; Road Vehicles—Functional Safety—Part 1: Vocabulary. International Organization for Standardization (ISO): Geneva, Switzerland, 2018.
73. *ISO 21448:2022*; Road Vehicles—Safety of the Intended Functionality. International Organization for Standardization (ISO): Geneva, Switzerland, 2022.
74. United Nations Economic Commission for Europe. UN Regulation No. 79—Uniform Provisions Concerning the Approval of Vehicles with Regard to Steering Equipment [2025/3]. *Off. J. Eur. Union* **2025**, *L*, 2025/3. Available online: https://eur-lex.europa.eu/eli/reg/2025/3/oj (accessed on 24 November 2026).
75. *ISO 23793-1:2024*; Intelligent Transport Systems—Minimal Risk Manoeuvre (MRM) for Automated Driving—Part 1: Framework, Straight-Stop and In-Lane Stop. International Organization for Standardization (ISO): Geneva, Switzerland, 2024.
76. Pan, T.; Chang, X.; Xiong, J.; Qiao, M. Fault-tolerant control of electric vehicles with multichannel quantization and actuator faults. *Int. J. Robust Nonlinear Control* **2026**, *36*, 4504–4516. [CrossRef]
77. Yu, M.; Wang, Z.; Wang, H.; Jiang, W.; Zhu, R. Intermittent fault diagnosis and prognosis for steer-by-wire system using composite degradation model. *IEEE J. Emerg. Sel. Top. Circuits Syst.* **2023**, *13*, 557–571. [CrossRef]
78. Zhou, S.; Li, Y.; Tong, S. Prescribed performance adaptive fuzzy output feedback control for steer-by-wire vehicle system with intermittent actuator faults. *Neural Comput. Appl.* **2024**, *36*, 16057–16070. [CrossRef]
79. Yang, J.; Yu, Y.; Zeng, D.; Hu, Y.; Liu, J.; Liu, K.; Carbone, G.; Luo, S.; Zhu, X. An adaptive sliding mode fault-tolerant control of variable speed reaching law for steer-by-wire systems. *Sci. Rep.* **2025**, *15*, 12846. [CrossRef] [PubMed]
80. Wang, K.; Qu, B.; Gao, M. Redundancy control strategy for a dual-redundancy steer-by-wire system. *Actuators* **2024**, *13*, 378. [CrossRef]
81. Li, H.; Zhang, N.; Wu, G.; Li, Z.; Ding, H.; Jiang, C. Active fault-tolerant control of a four-wheel independent steering system based on the multi-agent approach. *Electronics* **2024**, *13*, 748. [CrossRef]
82. Zhang, H.; Jiang, W.; Zhao, W.; Li, Y. Tracking and fault-tolerant controller design for uncertain steer-by-wire systems using model predictive control. *Chin. J. Mech. Eng.* **2024**, *37*, 141. [CrossRef]
83. Zhu, S.; Lu, J.; Zhu, L.; Chen, H.; Gao, J.; Xie, W. Coordinated control of differential drive-assist steering and direct yaw moment control for distributed-drive electric vehicles. *Electronics* **2024**, *13*, 3711. [CrossRef]
84. Jeong, Y. Model predictive control based integrated fault tolerant controller for autonomous vehicles with four-wheel independent steering, driving and braking systems. *Veh. Syst. Dyn.* **2025**, *63*, 2062–2085. [CrossRef]
85. Wu, X.; Wei, C.; Tian, H.; Wang, W.; Jiang, C. Fault-tolerant control for path-following of independently actuated autonomous vehicles using tube-based model predictive control. *IEEE Trans. Intell. Transp. Syst.* **2022**, *23*, 20282–20297. [CrossRef]
86. Chen, X.; Jiang, R.; Zhao, W.; Wang, C. Tube-based cooperative robust control for distributed drive electric vehicles suffering actuator faults. *IEEE Trans. Transp. Electrif.* **2025**, *11*, 3502–3513. [CrossRef]
87. Lee, J.; Hwang, Y.; Choi, S.B. Robust tube-MPC based steering and braking control for path tracking at high-speed driving. *IEEE Trans. Veh. Technol.* **2023**, *72*, 15301–15316. [CrossRef]
88. Li, Y.; Chen, Q.; Zhang, T.; Wang, J. Path following fault-tolerant control of distributed drive autonomous unmanned vehicle via adaptive terminal sliding mode. *J. Frank. Inst.* **2024**, *361*, 429–452. [CrossRef]
89. Xu, H.; Zhou, J.; Li, X.; Zhao, X.; Liu, Y. Fixed-time adaptive fault-tolerant control with guaranteed-performance using differential steering for 4WID vehicle considering steering actuator failure. *Proc. Inst. Mech. Eng. D J. Automob. Eng.* **2026**, *ahead of print*. [CrossRef]
90. Chen, H.; Tu, Y.; Wang, H.; Shi, K.; He, S. Fault-tolerant tracking control based on reinforcement learning with application to a steer-by-wire system. *J. Frank. Inst.* **2022**, *359*, 1152–1171. [CrossRef]
91. Deng, H.; Zhao, Y.; Nguyen, A.-T.; Huang, C. Fault-tolerant predictive control with deep-reinforcement-learning-based torque distribution for four in-wheel motor drive electric vehicles. *IEEE/ASME Trans. Mechatron.* **2023**, *28*, 668–680. [CrossRef]
92. Han, J.; Zhang, J.; Zhao, S.; Han, Z.; Jiang, Y.; Wei, H. Path replanning and hybrid fault tolerant control for intelligent vehicle under steering system faults. *IEEE Trans. Consum. Electron.* **2026**, *72*, 3819–3829. [CrossRef]
93. Cakmakci, M.; Koysuren, M.K. A computationally efficient control allocation method for four-wheel-drive and four-wheel-independent-steering electric vehicles. In Proceedings of the 2022 American Control Conference (ACC), Atlanta, GA, USA, 8–10 June 2022; pp. 3044–3049. [CrossRef]
94. Lu, A.; Li, R.; Yu, Y.; Tian, G. Unveiling four key factors for tire force control allocation in 4WID-4WIS electric vehicles at handling limits. *Proc. Inst. Mech. Eng. D J. Automob. Eng.* **2026**, *240*, 1788–1804. [CrossRef]

95. Senoussi, M.A.; Puig, V.; Boumehraz, M.; Sentouh, C.; Glida, H.E. Fault-tolerant control of autonomous vehicles using LPV-MPC and direct yaw moment compensation for steering failures. In Proceedings of the 2025 11th International Conference on Control, Decision and Information Technologies (CoDIT), Split, Croatia, 15–18 July 2025; pp. 2208–2213. [CrossRef]
96. Li, J.; Yang, C.; Fang, J.; Zhang, Y. A fault-tolerant trajectory tracking strategy of four-wheel independent drive electric vehicles using super-twisting sliding model control. *IEEE Trans. Transp. Electrif.* **2025**, *11*, 3907–3917. [CrossRef]
97. Wang, Q.; Ren, Z.; Cui, C.; Jiang, G. The study of multi-objective adaptive fault-tolerant control for in-wheel motor drive electric vehicles under demagnetization faults. *Actuators* **2026**, *15*, 44. [CrossRef]
98. Chen, T.; Cai, Y.; Chen, L.; Xu, X.; Sun, X. Trajectory tracking control of steer-by-wire autonomous ground vehicle considering the complete failure of vehicle steering motor. *Simul. Model. Pract. Theory* **2021**, *109*, 102235. [CrossRef]
99. Han, J.; Zhang, J.; Lv, C.; He, C.; Wei, H.; Zhao, S. Robust fault tolerant path tracking control for intelligent vehicle under steering system faults. *IEEE Trans. Intell. Veh.* **2025**, *10*, 244–254. [CrossRef]
100. Lee, J.; Choi, S.B. Integrated control of steering and braking for path tracking using multi-point linearized MPC. *IEEE Trans. Intell. Veh.* **2023**, *8*, 3324–3335. [CrossRef]
101. Oh, S.; Kim, H.; Jang, M.; Lee, J.; Oh, K.; Yi, K. Sliding mode approach for partitioned cost function-based fault-tolerant control of automated driving. In Proceedings of the 2021 21st International Conference on Control, Automation and Systems (ICCAS), Jeju, Republic of Korea, 12–15 October 2021; pp. 1732–1736. [CrossRef]
102. Zhang, B.; Lu, S.; Wu, W.; Li, C.; Lu, J. Robust fault-tolerant control for four-wheel individually actuated electric vehicle considering driver steering characteristics. *J. Frank. Inst.* **2021**, *358*, 5883–5908. [CrossRef]
103. Zhao, W.; Wang, A.; Zou, S.; Zhang, H. Individual auxiliary and fault-tolerant control of steer-by-wire system considering different drivers steering characteristics. *IEEE/ASME Trans. Mechatron.* **2021**, *26*, 1558–1569. [CrossRef]
104. Zhang, B.; Lu, S.; Xie, W. Cooperative game-based driver assistance control for vehicles suffering actuator faults. *IEEE Trans. Intell. Transp. Syst.* **2022**, *23*, 8114–8125. [CrossRef]
105. Zhang, B.; Lu, S.; Xie, F.; Xie, W. Stochastic cooperative game-based assistant fault-tolerant control considering driver behavior uncertainty. *IEEE Trans. Transp. Electrif.* **2022**, *8*, 2595–2607. [CrossRef]
106. Zhang, B.; Ji, J.; Ren, Y.; Yu, Y. Koopman game-based robust fault-tolerant control of steer-by-wire systems under driver-automation interaction. *Control Eng. Pract.* **2025**, *165*, 106532. [CrossRef]
107. Zhang, B.; Ji, J.; Ren, Y.; Zhao, Y.; Kan, Y. Neural network Nash game-based driver assistance fault-tolerant control for steer-by-wire systems. *IEEE Trans. Transp. Electrif.* **2025**, *11*, 7120–7130. [CrossRef]
108. Guo, J.; Luo, Y.; Li, K. Robust H∞ fault-tolerant lateral control of four-wheel-steering autonomous vehicles. *Int. J. Automot. Technol.* **2020**, *21*, 993–1000. [CrossRef]
109. Chang, Y.; Hu, M.; Yang, Z.; Bian, Y.; Lei, Z.; Qin, H. Active fault-tolerant path tracking control for autonomous vehicles considering actuator fault and model mismatch. *Control Eng. Pract.* **2025**, *162*, 106362. [CrossRef]
110. Xiao, F.; Jiang, Y.; Cheng, R.; Xu, C.; Tang, X.; Gao, F.; Li, J. Steering system fault diagnosis and fault-tolerant control of active wheel-corner electric vehicles. *SAE Int. J. Veh. Dyn. Stab. NVH* **2026**, *10*, 10-10-04-0036. [CrossRef]
111. Lu, A.; Li, R.; Xu, Y.; Tian, G. Adaptive fault-tolerant control for 4WID-4WIS electric vehicles under steering system failures. In Proceedings of the 2024 36th Chinese Control and Decision Conference (CCDC), Xi'an, China, 25–27 May 2024; pp. 443–448. [CrossRef]

Disclaimer/Publisher's Note: The statements, opinions and data contained in all publications are solely those of the individual author(s) and contributor(s) and not of MDPI and/or the editor(s). MDPI and/or the editor(s) disclaim responsibility for any injury to people or property resulting from any ideas, methods, instructions or products referred to in the content.